Protective effect of starch-stabilized selenium nanoparticles against melamine-induced hepato-renal toxicity in male albino rats

Zainab Sabry Othman Ahmed[1], Mona K. Galal[2], Elsayed A. Drweesh[3], Khaled S. Abou-El-Sherbini[3], Eman A.M. Elzahany[3], Mohamed M. Elnagar[*3,4], Noha A. E. Yasin[*1]

[1] Cytology and Histology Department, Faculty of Veterinary Medicine, Cairo University, Giza 12211, Egypt.

[2] Biochemistry and Chemistry of Nutrition Department, Faculty of Veterinary Medicine, Cairo University, Giza 12211, Egypt.

[3] Inorganic Chemistry Department, National Research Centre, 33 El Bohouth St. (former Eltahrir St.), Dokki, Giza 12622, Egypt.

[4] Institute of Electrochemistry, Ulm University, Albert-Einstein-Allee 47, 89081 Ulm, Germany

[*]**Corresponding author:**

Mohamed M. Elnagar

Inorganic Chemistry Department, National Research Centre, 33 El Bohouth St. (former Eltahrir St.), Dokki, Giza 12622, Egypt.

Institute of Electrochemistry, Ulm University, Albert-Einstein-Allee 47, 89081 Ulm, Germany

E-mail address: mohamed.elnagar@uni-ulm.de; m.elnagar1@yahoo.com

Noha A. E. Yasin

Cytology and Histology Department, Faculty of Veterinary Medicine, Cairo University, Giza 12211, Egypt.

E-mail address: nohayassin428@cu.edu.eg; nohayassin428@yahoo.com

Phone number: +201155833448

Abstract

Melamine and its analogues are illegally added to raise the apparent protein content in foods. The elevated concentrations of these compounds cause adverse effects in humans and animals. In this contribution, the protective effects of the synthesized starch-stabilized selenium nanoparticles (Se-NPs@starch) on melamine-induced hepato-renal toxicity have been systematically investigated. The Se-NPs@starch were characterized by X-ray photoelectron spectroscopy (XPS) analysis, energy dispersive spectroscopy (EDS) mapping analysis, TEM, and FT-IR. Starch plays a crucial role in the stabilization and dispersion of Se NPs, as noticed from the TEM and EDS investigations. Furthermore, the atomic ratio of Se distribution over the starch surface is approximately 1.67%. The current study was conducted on four groups of adult male rats, and the oral daily treatments for 28 days were as follows: group I served as control, group II received Se-NPs@starch, group III was exposed to melamine, while group IV was treated with melamine and Se-NPs@starch. The results reveal a significant alteration in the histoarchitecture of both hepatic and renal tissues induced by melamine. Furthermore, elevated liver and kidney function markers, high malondialdehyde, and increased expression levels of apoptosis-related genes besides a reduction in GSH and expression levels of antioxidant genes were observed in the melamine-exposed group. Interestingly, the administration of the Se-NPs@starch resulted in remarkable protection of rats against melamine-induced toxicity through increasing the antioxidant capacity and inhibiting oxidative damage. Collectively, this study provides affordable starch-stabilized Se-NPs with potent biological activity, making them auspicious candidates for prospective biomedical applications.

Keywords:

Melamine-toxicity; Liver, Kidneys; Se-NPs@starch; Immobilization.

1. Introduction

Melamine is frequently used in different products as furniture, laminates, plastics, food utensils, coatings, glues, commercial filters, and dining ware [1]. Melamine intake at very low concentrations is harmless for animals because it is hardly metabolized by animals and rapidly eliminated via urine (more than 90%) [2]. Furthermore, World Health Organization (WHO) and U.S. Food & Drug Administration (USFDA) determined the safe level of melamine concentration in human food materials to be 2.5 mg/kg [3]. However, melamine and its analogues, such as nitrogen-rich triazine compounds, are illegally added to various foodstuffs to falsify the protein contents, resulting in fatal adverse effects in children and pets [4]. Recently, exposed dairy products containing melamine have raised concerns regarding its toxicity [5, 6]. For example, nephrotoxicity was noticed among the children who ingested milk- infant formula contaminated with melamine [7]. Unfortunately, this outbreak was accompanied by urinary stones in both infants and children. As a consequence, 294,000 of them were influenced with more than 50,000 hospitalized and 6 died due to acute renal failure [8]. Besides, renal failure and death were reported in domesticated dogs and cats after exposure to pet food contaminated with melamine and its analogs [9-11].

Melamine can accumulate in the brain, liver, spleen, and bladder as an effect of oral administration over time [12]. Elevated concentrations of melamine in these organs induce adverse effects on the growth of fetuses and neonates [13]. Likewise, ingestion of melamine leads to sperm abnormalities and DNA damage [14], in addition to detrimental impacts on the male reproductive system [15].

Testicular damage is observed to be associated with oxidative stress [16]. Oxidative stress is a pathophysiological phenomenon that emerges from the imbalance between the formation of reactive oxygen species (ROS) and the anti-oxidative efficiency of the enzymatic and non-enzymatic antioxidants [17]. Excessive ROS can cause alterations in the cellular macromolecules including lipids, proteins, and DNA, followed by a disruption of the cell wall, cellular enzymes inactivation, and eventually cell death [18, 19]. On that front, substantial efforts have been devoted to inhibiting melamine toxicity [20, 21].

Metal nanoparticles are of utmost importance in medicine and pharmacology due to their fascinating properties such as chemical stability, non-toxicity, and biocompatibility [22, 23]. Among them, selenium (Se) is a fundamental trace element required for the regular physiological function of growing animals [24] and is obtained from plants. Besides, Se is very important to human health because of its potent pro-oxidant, and antioxidant effects, anti-inflammatory, and immunity-boosting capabilities [25, 26]. Remarkably, many Se compounds are reported to have significant anti-cancer activity and chemopreventive properties [27]. More outstandingly, Se NPs show an antiviral effect against the current pandemic of SARS-CoV-2 (coronavirus disease 2019), which has been confirmed using Ebselen [26]. However, there is a very narrow boundary between the acceptable concentrations of Se intake and its toxicity [28]. Generally, the pro-oxidant and antioxidant effects, bioavailability, and toxicity of Se are strongly affected by its chemical form, particle size, and concentration. These properties are crucial to determine the interaction of Se with biological entities [29]. For example, the toxicity of Se is remarkably inhibited in the nano-size zerovalent form. Moreover, Se-NPs with particles size of 5–200 nm can efficiently scavenge free radicals such as superoxide anion and 1,1-diphenyl-2-picrylhydrazyl (DPPH) [30]. While selenomethionine is a very safe natural source of Se with high bioavailability, lower toxicity

accompanied with a similar ability to increase selenoenzyme levels were detected for Se-NPs of average particle size of 36 nm [31]. Zhang et al. showed that the toxicity of Se-NPs in mice is seven times lower than that of sodium selenite and three times lower than that of organic Se compounds [32]. Additionally, nanoparticle applications in the fisheries and livestock world revealed that Se-NPs enhance the efficacy of growth, digestion, immunomodulation, and reproduction [33] as well as increase the productivity of stress-ridden fish and livestock [34].

Despite the fascinating properties of NPs, they suffer from aggregation in suspensions due to their high surface energy, consequently, their activity sharply declines as a function of time [35]. Hence, to control the dispersion and size of Se-NPs, natural polysaccharides like chitosan [36], and cellulose [37] were used as natural stabilizers and size controlling agents. One should emphasize that the shelf-life storage of the stabilized metal nanoparticles via the immobilization approach is extremely long and can exceed 5 years [35].

In continuation of our previous work on Se-NPs and their interesting aspects [38], starch-stabilized Se-NPs (Se-NPs@starch) were synthesized and characterized by XPS, FT-IR, and TEM. The potential activity of the synthesized starch-stabilized Se-NPs was evaluated for inhibiting the toxicity of hepatic and renal tissues induced by melamine ingestion. The experiments were conducted on four groups of male albino rats including group I (control), group II received starch-stabilized Se-NPs, group III received melamine, whereas group IV received both melamine and starch-stabilized Se-NPs. Statistical analysis of the results is also provided.

2. Materials and methods

2.1. Chemicals and reagents

Melamine ($C_3H_6N_6$, LOBA Chemie, India) was obtained from El-Mekkawy Company, Cairo. Selenium (Sigma-Aldrich, CAS 7782-49-2 034-001-00-2), potato starch (CAS Number: 9005-25-8), ascorbic acid (CAS Number: 50-81-7), and nitric acid (HNO_3, CAS Number 7697-37-2) were of high-purity grade from Sigma–Aldrich.

2.2. Methods

2.2.1. Selenous acid preparation

0.050 M of selenous acid (H_2SnO_3) was prepared by dissolving 0.987 g of Se metal in concentrated HNO_3 before heating till dryness and dissolved in 250 mL distilled water [38].

2.2.2. Synthesis of selenium nanoparticles impregnated on starch (Se-NPs@starch)

Se-NPs were synthesized by a versatile and green procedure using starch as a stabilizer, and ascorbic acid as a reducing agent that reduces Se (IV) to Se. Se-NPs are stabilized by starch according to the literature but with replacing cellulose with starch [38, 39]. In detail, the selenous acid/starch aqueous solution was prepared as follows: 50.0 g potato starch was boiled in 100 mL water and then mixed with 250 mL of 0.05 M selenous acid before completing the total volume to 800 mL. Afterward, 100 mL of 0.20 M ascorbic acid solution was added dropwise into the selenous acid/starch solution to start the reduction reaction. After the addition of ascorbic acid, the solution changed from transparent to red, indicating the formation of Se-NPs. The obtained crimson red solution was concentrated to less than 100 mL using a rotary evaporator at 80 °C. A crimson red

gel is formed, which is dried at 80 °C in an oven to produce shiny crimson red particles (Se-NPs@starch). The synthesized Se-NPs@starch was characterized by X-ray photoelectron spectroscopy (XPS), Fourier-transform infrared (FTIR), and Transmission Electron Microscope (TEM).

2.3. Instrumentation

To investigate the surface chemical composition and oxidation state of Se, X-ray photoelectron spectroscopy (XPS) analysis was conducted using a UHV Multiprobe system (Scienta Omicron, Germany) with a monochromatic X-ray source (Al Kα) and an electron analyzer (Argus CU) with 0.60 eV energy resolution. Fourier-transform infrared (FTIR) spectra were recorded on a Nicolet iS10, Thermo-Fisher Scientific, USA, using a KBr pellet. The TEM images of Se-NPs@starch were obtained by a TEM of the Se-NPs@starch using a JEOL model 1200EX electron microscope at an operating voltage of 120 kV.

2.4. Experimental protocol and animal grouping

2.4.1. Experimental animals and ethical approval

Adult male albino rats (n= 40, average B.W= 200±20 g) were kept in plastic cages under the standard hygienic conditions (60% relative humidity, 24 ± 3°C room temperature, and 12: 12- h light: dark cycle with *ad libitum* access to food and drinking water). Rats were treated humanely according to NIH guidelines, and the experimental procedure was accepted by the Institutional Animal Care and Use Committee (IACUC) of the Faculty of Veterinary Medicine, Cairo University (Approval number Vet CU28042021291).

2.4.2. Experimental design

Rats were acclimated for one week, then they were assigned to 4 equal groups of ten each (n=5 rats/cage); group I (untreated control group) only received distilled water, Group II: Se-NPs@starch treated group (2 mg Se-NPs/kg) as previously mentioned by Rezvanfar et al. [40], group III: melamine-treated group (300 mg/kg) as previously reported by An et al. [41], and group IV: Se-NPs@starch co-treated group (received melamine (300 mg/kg) plus Se-NPs (2 mg/kg)). All treatments were received daily by stomach tube for 28 days.

2.5. Sample collection and preparation

After 28 days of treatment, serum samples were obtained from rats for measuring the function of both liver and kidney. Then, rats were euthanized by cervical dislocation for collection of the liver and kidney samples. Some specimens of these organs were stored at -80 °C for estimation of oxidative stress biomarkers in their tissue homogenates and quantitative real-time PCR (Rt-PCR) analysis for some antioxidant- and some apoptotic- related genes, while other specimens were histopathologically and immunohistochemically investigated after fixation in 10% neutral-buffered formalin (NBF) solution.

2.6. Biochemical analysis

2.6.1. Determination of Liver Function Markers

The activities of both serum aspartate- and alanine- aminotransferase (AST & ALT) were assayed using reagent kits (Spectrum Diagnostics Co., Egypt) following the provided instructions.

2.6.2. Determination of kidney Function Markers

The levels of serum creatinine and urea were assayed using reagent kits (Spectrum Diagnostics Co.) following the provided instructions.

2.6.3. Hepatic and renal oxidative stress biomarkers

A Teflon tissue homogenizer was used to homogenize both liver and kidney samples in 10% (W/V) ice-cold 0.1 M phosphate buffer saline (PBS) (pH 7.4). Crude tissue homogenate was centrifuged at 15,000 rpm for 15 min at 4 ºC and subsequently used for determination of reduced glutathione (GSH) content as previously mentioned by Ellman [42], malondialdehyde (MDA) content according to Ohkawa et al. [43], in addition to total protein concentration as previously reported by Bradford [44].

2.6.4. qRT-PCR analysis for Nrf-2, GP_X, c-Myc, and CASP 3 genes

The relative hepatic and renal Nrf-2, GP_X, c-Myc, and CASP 3 mRNA abundance was determined by qRT-PCR analysis using GAPDH as a housekeeping gene. Total RNA was extracted from approximately 100 mg liver and kidney tissues using the total RNA Extraction Kit (Vivantis, Malaysia). By using M-MuLV Reverse Transcriptase (NEB#M0253). RT-PCR was carried out after confirming the concentration and purity of RNA. By fluorescence-based real-time detection method with a fluorescent SYBR Green dye (Thermo Scientific, Cat. No. K0221), a quantitative assessment of cDNA amplification for each gene was performed. The primer sequence used for RT-PCR analysis is shown in **Table 1.** The real-time PCR conditions were carried out as follow: 95 ºC for 5 min (initial denaturation) and then 40 cycles at 95 ºC for 15 s, 60 ºC for 30 s, and 72 ºC for 30 s in each experiment. Negative controls that were free of the template were included.

Each qRT-PCR was performed with three biological replicates, and each biological replicate was assessed three times. Using the comparative $2^{-\Delta\Delta CT}$ method, the relative transcription levels were calculated [45].

Table 1. Primer sequence used for qRT-PCR.

Gene symbol	Gene description	Accession number	Primer Sequence
GAPDH	Glyceraldehyde3-phosphate dehydrogenase	NC_005103.4	F:- 5′-ACCACAGTCCATGCCATCAC-3′ R:- 5′-TCCACCACCCTGTTGCTGTA-3′
Nrf 2	Nuclear factor, erythroid 2-like 2	NC_005102.4	F: -5′-GGCCCTCAATAGTGCTCAG-3′ R:-5′-TAGGCACCTGTGGCAGATTC-3′
GP_X	Glutathione peroxidase	M21210.1	F:- 5′-CTCTCCGCGGTGGCACAGT-3′ R:- 5-CCACCACCGGGTCGGACATAC-3
c-Myc	Cytochrome c	K00750.1	F:- 5′-TAC CC T CTC AAC GAC AGC AG-3′ R:- 5′-TCT TGA CAT TCT CCT CGG TG-3′
CASP 3	Caspase 3	NM_012922.2	F: -5′-GGAGCTTGGAACGCGAAGAA-3′ R:-5′-ACACAAGCCCATTTCAGGGT-3′

2.7. Histopathology

2.7.1. Light microscopy (L.M.)

Both liver and kidney specimens collected from the four groups were immediately fixed for 48-72 h in 10% NBF, embedded in increasing grades of alcohol. Then, tissue specimens were cleared with xylene and fixed in paraffin. 3-4 μm paraffin sections were processed for staining with hematoxylin and eosin (H&E) for histopathological investigation as described by Bancroft and Gamble [46].

All the noticeable histopathological alterations in the liver and kidneys were graded using a classical semiquantitative scoring system to assess the degree of lesion severity between different groups (n= 5 slides representing 5 rats per group) as follows: (0) none (normal histology) while (1), (2), (3) and (4) indicate mild <25%, moderate 25%-50%, severe 50%-75%, and extensive severe >75% tissue damage, respectively [47]. The main histopathological parameters used for liver injury were congestion, vacuolar degeneration, and inflammation while, those for renal damage were tubular degeneration and necrosis, glomerular atrophy, congestion, and hyalinization.

2.7.2. Immunohistochemical analysis

Immunohistochemistry was carried out on deparaffinized hepatic and renal sections (4-μm thick) for detection of apoptosis according to the manufacturer's protocol. Sections were immersed in 0.3% hydrogen peroxide (H_2O_2) in phosphate-buffered saline (PBS) for 20 min for deactivation of endogenous peroxidase, incubated with rabbit polyclonal anti-caspase-3 antibodies (active/cleaved) (100-56113, Novus biologicals) 1:100 for 1hr then washed out. After that, tissue sections were incubated for 20 min with secondary antibody Horse Radish peroxidase (HRP) Envision Kit (DAKO), washed out, and incubated for 10-15 min with diaminobenzidine (DAB). Sections were washed, counterstained in hematoxylin, dehydrated in alcohol, cleared with xylene, and covered with a coverslip for microscopic examination.

Caspase 3 -stained liver and kidney sections were assessed using Leica Quin 500 software (Leica Microsystems, Switzerland) for morphological analysis. Caspase 3 immunostaining was quantified as area percentage in different slides (n=5 fields/group) at magnification power x400.

The areas displaying brown color immunoreaction (positive) were selected for estimation. Mean values and standard error mean (SEM) of each specimen were obtained and statistically analyzed.

2.8. Statistical analysis

Descriptive statistics were presented as mean ± SEM. The obtained results were subjected to one-way analysis of variance (ANOVA) using SPSS version 25.0 software (IBM, USA) followed by Tukey post hoc test. Data were considered significantly different at *P*-value less than 0.05.

3. Results

3.1. Characterization

XPS investigations were performed to identify the surface chemical composition of Se-NPs@starch and the valence state of Se. **Fig. 1a** shows the XPS spectra (survey) of the Se-NPs@starch sample. From the survey spectra, the peaks corresponding to Se, O, and C are observed. The high-resolution spectrum of Se implies the peaks of Se $3d_{5/2}$ and Se $3d_{2/3}$ at approximately 55.6 and 56.6 eV, respectively confirming the presence of elemental selenium (Se^0), as shown in **Fig. 1b.** Furthermore, the absence of Se 2p, 2s, and 1s peaks indicates that Se (IV) was entirely reduced during the synthesis of the Se-NPs@starch [48]. Besides Se^0, the sample contained organic material on the surface as revealed by the presence of C, and O **(Fig. 1c)**. The C 1s peak in the XPS spectrum of starch has been deconvoluted into three peaks at 284.80, 286.4, and 288.7 eV, as presented in **Fig. 1c** [49].

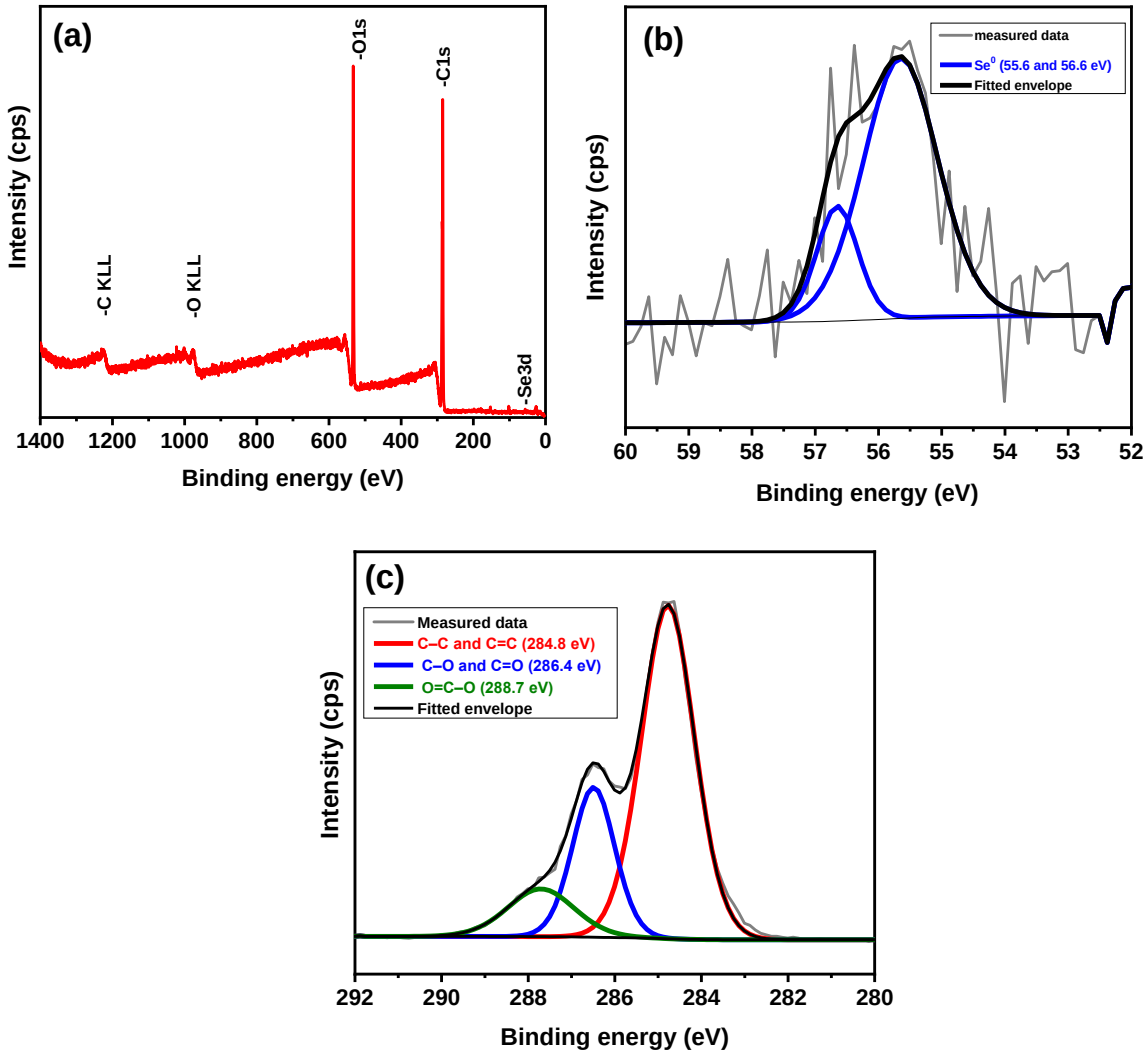

Fig. 1. (a-c) XPS analysis of Se-NPs@starch. The spectra are fitted with a linear combination of the corresponding reference spectra.

The FTIR spectra of the Se-NPs@starch and starch were measured in the range of 400–4000 cm^{-1}, as shown in **Fig. 2.** The bands observed in both spectra at around 3260 cm^{-1}, 2931 $cm^{-1,}$ and 1635 cm^{-1}, are correlated to O-H stretching vibration, C-H stretching, and C-O bending vibration associated with the OH group, respectively [50]. The presence of Se-NPs connected to starch is confirmed by a red-shift of about 5 cm^{-1} for OH stretching vibration as well as the band at 763

cm^{-1} [51]. Additionally, a very clear band of Se-NPs at 643 cm^{-1} is noticed in the spectrum which is characteristic of the spherical shape of Se-NPs [52-54].

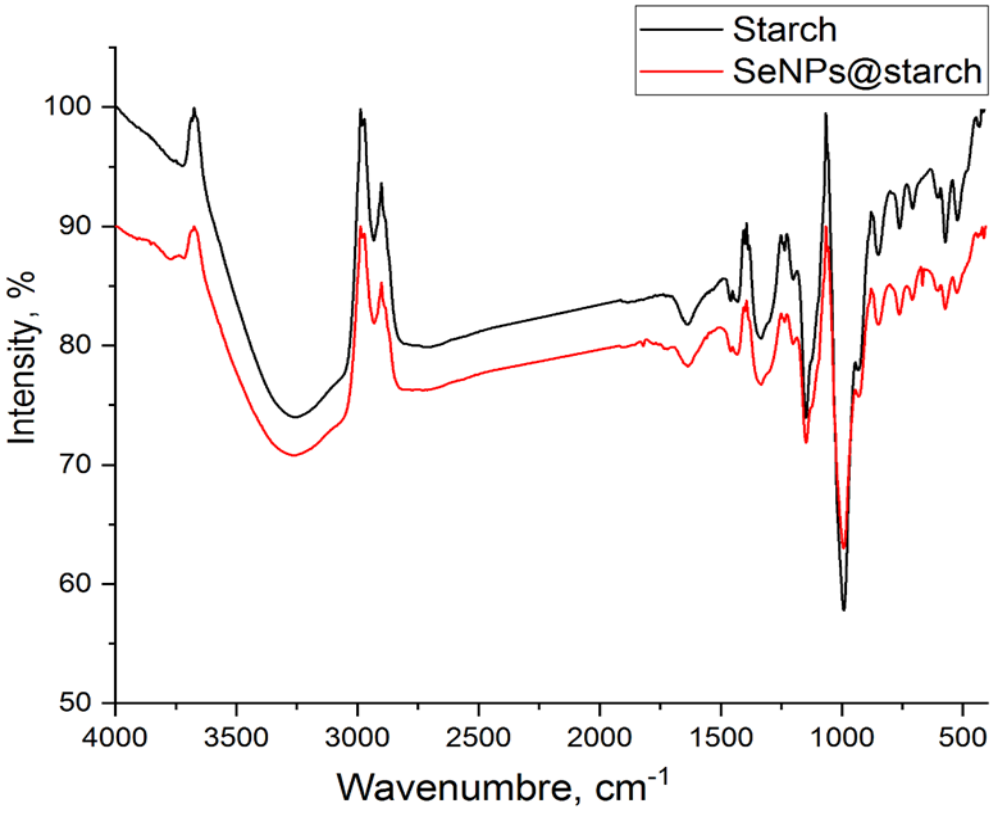

Fig. 2. FTIR spectrum of the Se-NPs@ starch compared with the free starch.

TEM micrographs of Se-NPs@starch **(Fig. 3a and 3b)** show Se-NPs in a dark spherical shape characterized by particle size ranging from 20 to 140 nm impregnated on starch. The energy dispersive spectroscopy (EDS) mapping analysis reveals the peaks corresponding to C, O, and Se confirming the successful synthesis of Se-NPs@starch, as shown in Figure 3c. Notably, **Fig. 3c** demonstrates that Se with an atomic mass of 1.67% is distributed homogeneously over the starch surface. This low concentration of Se immobilized on starch is beneficial for biological applications since there is a very narrow boundary between the acceptable concentrations of Se

intake and its toxicity. Furthermore, the homogenous distribution of Se-NPs over the starch surface indicates the potential ability of starch to stabilize Se-NPs against agglomeration.

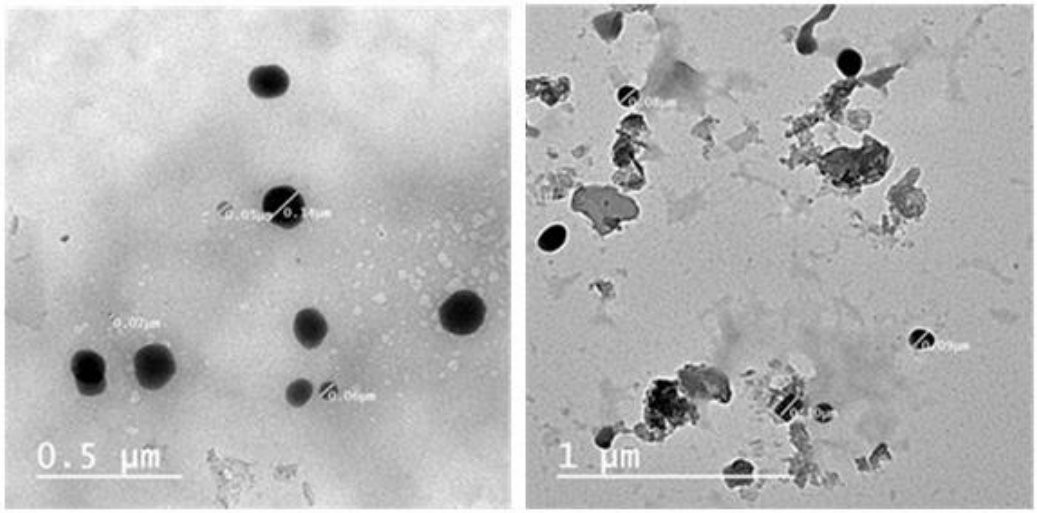

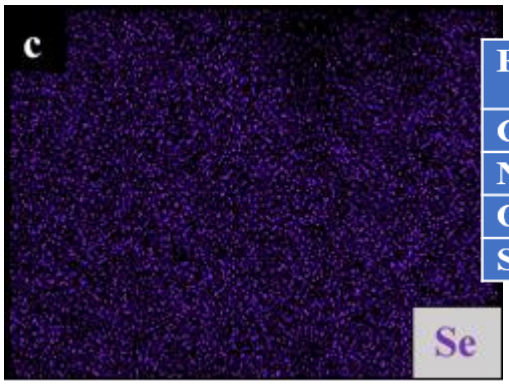

Element	Atomic%
C K	50.86
N K	2.70
O K	44.76
Se L	1.67

Fig. 3. (a and b) TEM images and (c) EDS elemental mapping of Se-NPs@ starch.

3.2. Liver and kidney functions

Hepatic damage was estimated by the determination of ALT and AST activities. **Fig. 4A** reveals that melamine significantly elevated the ALT activity from 41.81 U/L to 92.14 U/L and the AST activity from 93.42 U/L to 105.22 U/L compared to the control. Co-treatment with Se-NPs@starch showed a remarkable reduction in the ALT activity to 47.33 and a non-significant decrease in the AST activity to 96.46 compared to the melamine-intoxicated group.

Renal damage was estimated by the determination of serum urea and creatinine levels. **Fig. 4B** indicates that melamine significantly increased the serum urea level from 14.84 to 22.48 mg/dL and creatinine level from 0.75 to 1.50 mg/dL compared to the control group. Co-administration of Se-NPs@starch did not significantly decrease the serum urea level to 18.96 mg/dL and significantly decreases the creatinine level to 0.84 mg /dL in contrast to the melamine-intoxicated group.

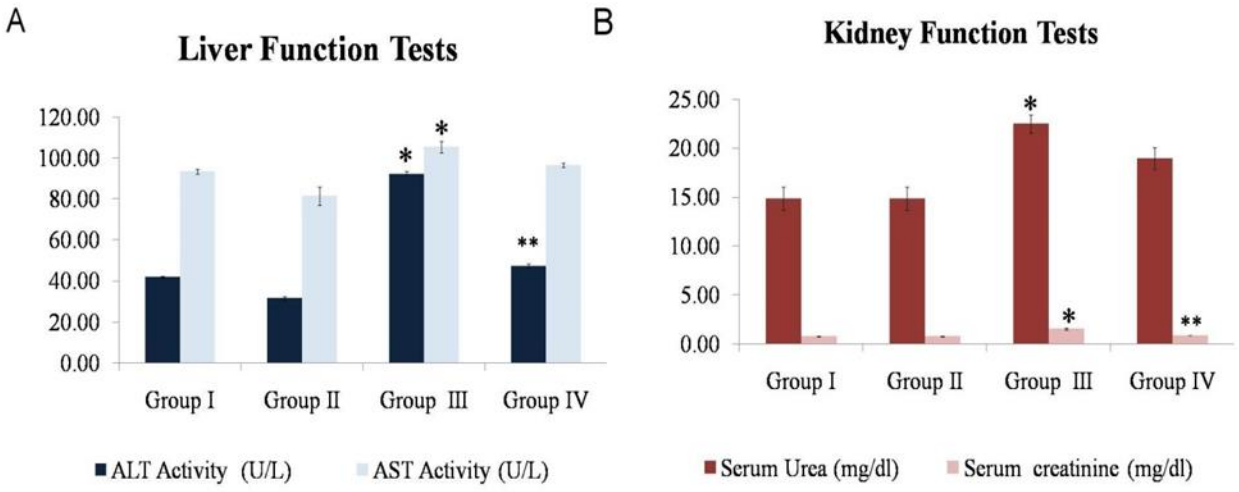

Fig. 4. Protective effects of Se-NPs against the melamine-induced hepatic (A) and renal (B) damage in male rats. Data are presented as the mean ± SEM. *indicates statistically different

from the control negative group ($p< 0.05$). ** indicates statistically different from the melamine-treated group ($p< 0.05$).

3.3. Hepatic and renal oxidative stress biomarkers

For studying the redox state of the cell, MDA (LPO biomarker) and some antioxidant machinery were evaluated.

3.3.1. Hepatic and renal MDA Content

Based on the results presented in **Fig. 5,** melamine markedly ($p< 0.05$) increased the hepatic and renal MDA level from 1.53 to 5.22 μM/mg and from 1.08 to 3.50 μM/mg protein, respectively, compared to the control group. Co-administration with Se-NPs@starch significantly declined both liver and kidney MDA contents to 2.30 μM/mg protein and 2.10 μM/mg protein, respectively, compared to the melamine-intoxicated group.

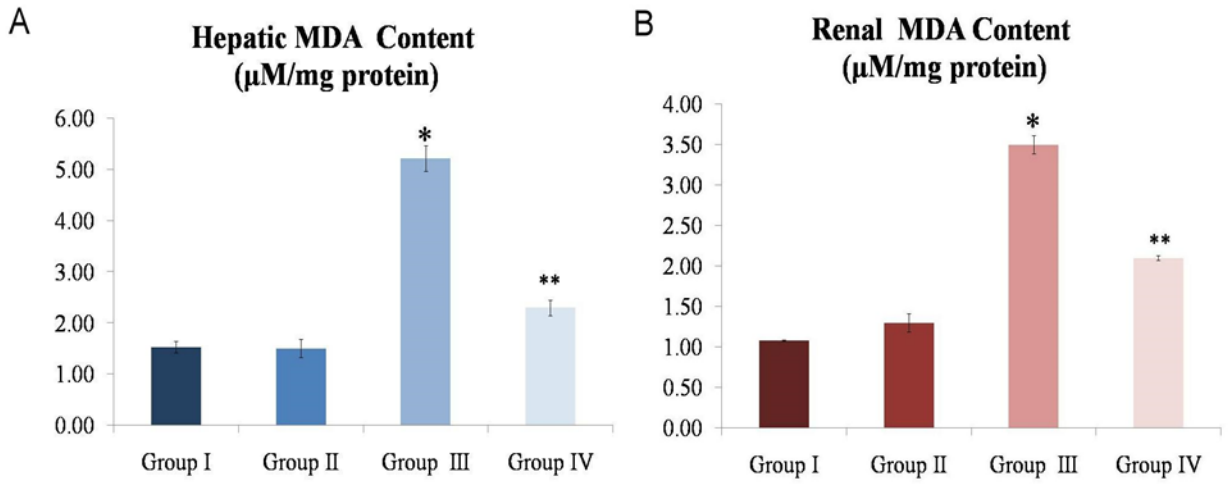

Fig. 5. Protective effects of Se-NPs against the melamine-induced high level of MDA (μM/mg protein) in albino rats. Data are presented as mean ± SEM. *indicates statistically different from

the control negative group ($p < 0.05$). ** indicates statistically different from the melamine-treated group ($p < 0.05$)

3.3.2. Antioxidant Machinery

Antioxidant Machinery was assessed by the determination of GSH content and mRNA relative expression for *Nrf-2* and *GPx* genes.

3.3.2.1. Hepatic and renal GSH content

Fig. 6 shows that melamine considerably depresses the hepatic and renal GSH content from 3.83 to 2.47 µM mg^{-1} and from 3.62 to 2.31 µM mg^{-1} protein, respectively, compared to the control group. Co-administration with Se-NPs@starch noticeably increased both liver and kidney GSH contents to 3.01µM/mg protein and 3.03 µM/mg protein, respectively compared to the melamine-intoxicated group.

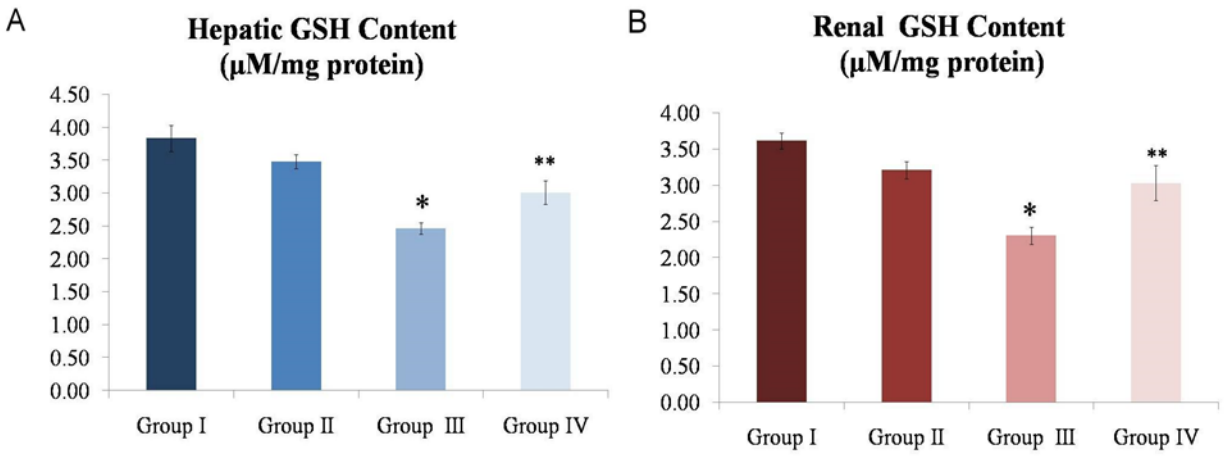

Fig. 6. Protective effects of Se-NPs against the melamine-induced reduction level of GSH (µM/mg protein) in albino rats. Data are presented as mean ± SEM. *indicates statistically

different from the control negative group ($p< 0.05$). ** indicates statistically different from the melamine-treated group ($p< 0.05$).

3.3.2.2. Hepatic and Renal mRNA relative expression for some antioxidant related genes (Nrf -2 and GPx)

For the melamine-intoxicated group, the *Nrf-2* gene was substantially downregulated to 0.28-fold and 0.16-fold compared to the control one in both liver and kidney tissues, respectively. While co-administration with Se-NPs@starch modulated the gene expression level to 0.71-fold in the liver and 0.40-fold in the kidney. Such alteration in the gene expression was significant when compared to the melamine-intoxicated group **(Fig. 7).** Furthermore, after exposure to melamine, the GP_X gene showed a considerable downregulation in both hepatic and renal tissues compared to the control one. Se-NPs@starch co-administration extensively elevated the expression level of the GP_X gene from 0.2 to 0.7-fold and from 0.2 to 0.82-fold for the liver and kidney tissues, respectively compared to the melamine-intoxicated group as shown in **Fig. 7**.

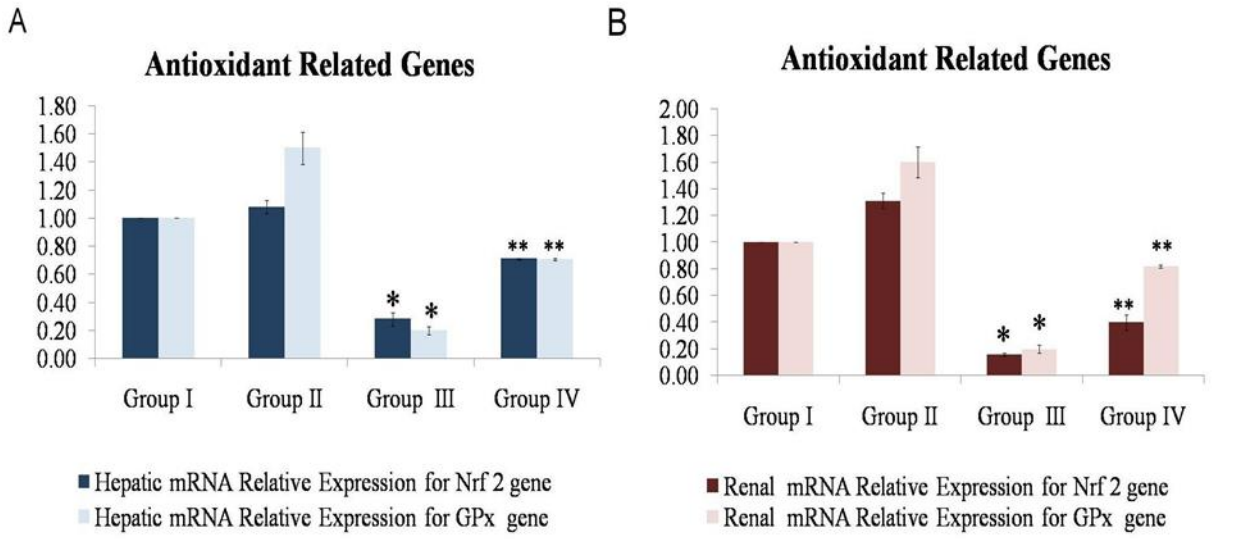

Fig. 7. Protective effects of Se-NPs against the melamine-induced downregulation of some antioxidant-related genes in male albino rats. (A) Hepatic *Nrf2* and *GPx* genes, **(B)** Renal *Nrf2* and *GPX* genes. Data are presented as mean ± SEM. *indicates statistically different from the control negative group ($p < 0.05$). ** indicates statistically different from the melamine-intoxicated group ($p < 0.05$).

4. Hepatic and Renal mRNA relative expression for some apoptotic-related genes (c-Myc and CASP 3)

Melamine expressively upregulated the c-Myc gene expression in both hepatic and renal tissues compared to the control group. In comparison, Se-NPs@starch co-administration significantly decreased the expression level of the c-Myc gene from 4 to 1.62-fold and from 6.20 to 1.8-fold in both liver and kidney, respectively as indicated in **Fig. 8.**

Compared to the negative control group, the expression level of the CASP 3 gene is dramatically upregulated in the melamine-intoxicated group, particularly in the kidney tissues. On the other hand, as shown in **Fig. 8**, Se-NPs@starch co-treatment significantly modulated the expression level of CASP 3 gene from 6.51 to 3.73 -fold and from 8.3 to 2- fold for both hepatic and renal tissues, respectively.

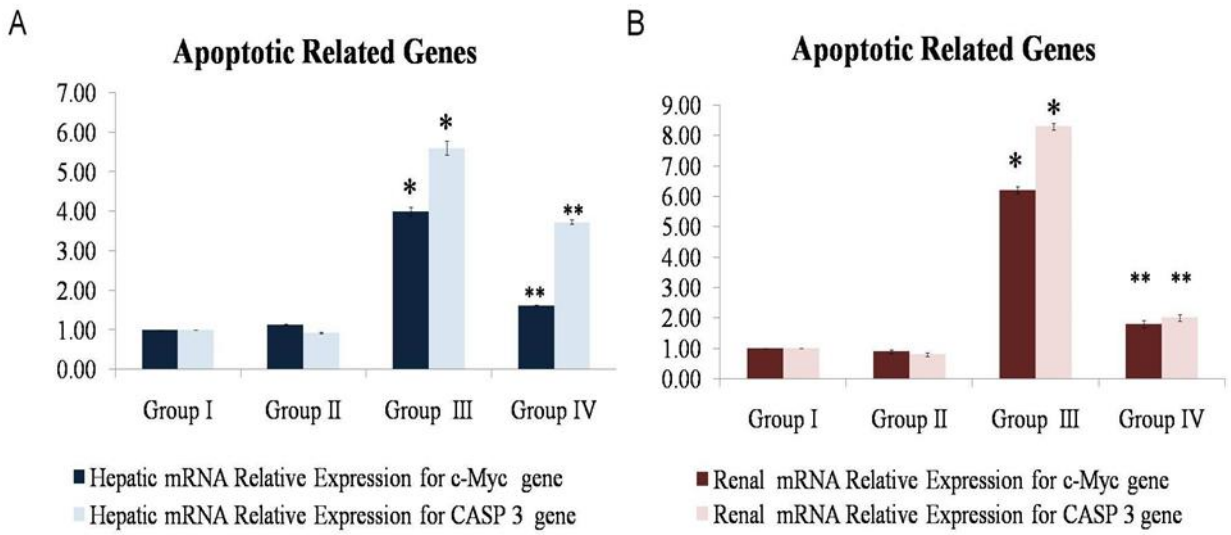

Fig. 8. Ameliorative effects of Se-NPs against the melamine-induced upregulation of some apoptotic-related genes in male albino rats. (A) Hepatic *c-Myc* and *CASP3 genes*, **(B)** Renal *c-Myc* and *CASP3 genes.* Data are presented as mean ± SEM *indicates statistically different from the control negative group ($p< 0.05$). ** indicates statistically different from the melamine-intoxicated group ($p< 0.05$).

5. Histopathological investigations

The microscopical examination of the hepatic sections obtained from the control group revealed a normal histological architecture of the liver that appeared with normal radiating cords of hepatocytes, normal central vein, and blood sinusoids **(Fig. 9a).** The Se-NPs@starch exposed group exhibited normal hepatocytes that appeared polyhedral with normal vesicular and central nuclei as well as arranged in hepatic cords that were radiating from the central vein. The hepatic cords were separated by normal blood sinusoids. In addition, the portal triad showed the normal histological structure of the bile duct and branches of the portal vein and hepatic artery **(Fig. 9b and 9c).** The hepatic tissues of the melamine-exposed rats had severe damage that was observed in the form of distortion of the hepatic cord's arrangement, edema, severe congestion, and

dilatation of the central vein. Blood sinusoids appeared severely dilated with clearly observable activated Von Kupffer cells. Furthermore, hepatocytes displayed severe ballooning and remarkable cytoplasmic vacuolization as well as different stages of degeneration and apoptosis. The dark brown deposition was also noticed inside the cytoplasm of hepatocytes. The portal area was disrupted, and the lining epithelium of the bile duct revealed distortion, in addition to inflammatory cells infiltration and severe congestion of the portal vein**,** as shown in **Fig. 9d-j.** On the other hand, the melamine-exposed group co-treated with Se-NPs@starch exhibited a partial recovery of the hepatic damage. The central vein appeared less congested with normal dilatation, while the blood sinusoids appeared with normal architecture. Some hepatocytes showed degeneration and ballooning with cytoplasmic vacuolization, but these alterations in the hepatic architecture were less in severity **(Fig. 9k, l)** in comparison to the melamine-exposed group.

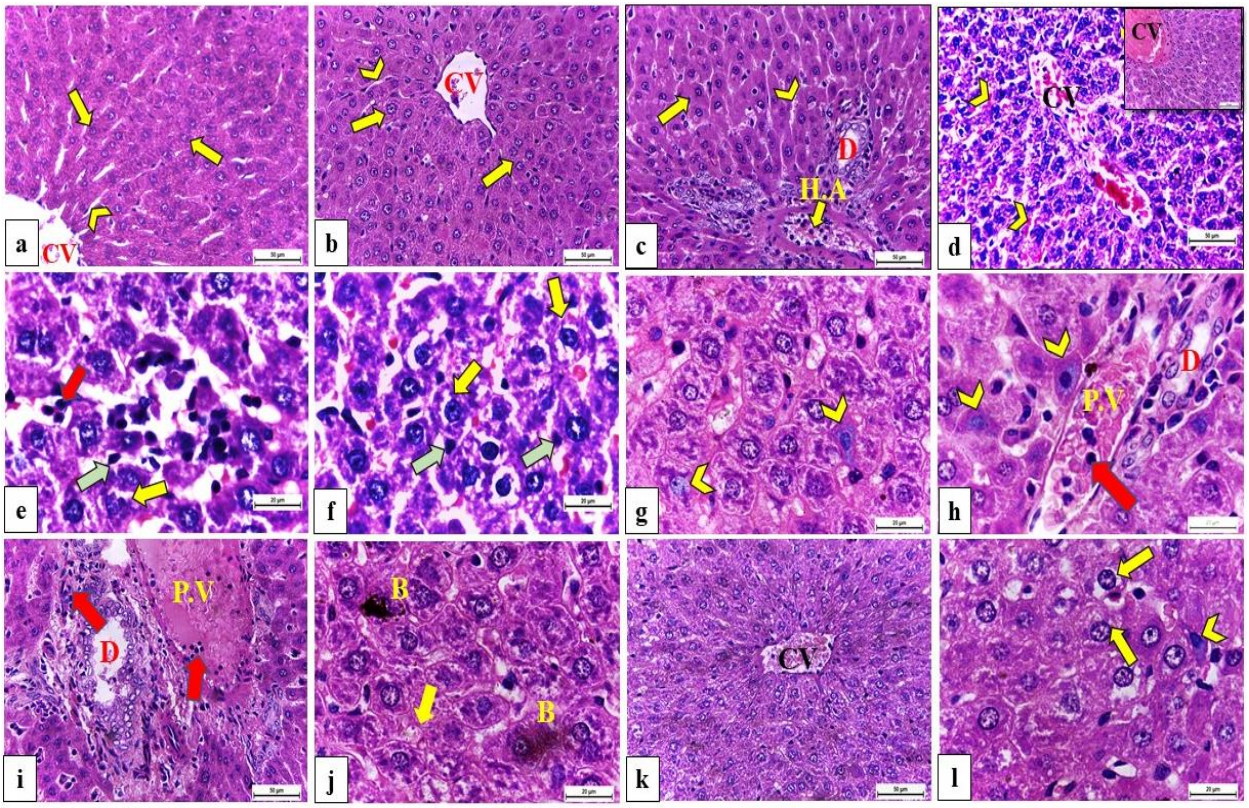

a: Control group; b, c: Nano-selenium group; d-j: Melamine group; k, l: Melamine and nano-selenium group.

Fig. 9. A photomicrograph of H&E-stained sections of rats' hepatic tissues showing: a (X400): The control group reveals normal cords of hepatocytes (arrow) that appeared radiating from a normal central vein (CV) and separated by normal hepatic sinusoids (chevron). The hepatocytes of the control group appeared polyhedral with central, vesicular, and spherical nuclei. **b, c (X400):** The nano-selenium exposed group exhibits normal architecture of the central vein (CV) and hepatocytes (arrow) separated by normal hepatic sinusoids (chevron). The portal area **(c)** shows an intact architecture of the bile duct (D) and branches of the portal vein and hepatic artery (H.A) **d-j:** The melamine-exposed group. **d (400X):** Hepatic tissue show distortion of hepatic cords arrangement, edema, severe congestion, and dilatation of the central vein (CV) and hepatic sinusoids (chevron). **e, f (X1000):** Blood sinusoids appear dilated with bulged activated Von Kupffer cells (green arrow), in addition to inflammatory cells infiltration (**e:** red arrow). Also, hepatocytes display ballooning and cytoplasmic vacuolization (yellow arrow). **g, h (X1000):** Different stages of hepatocyte degeneration and necrosis are seen (chevron). **h, i (X1000):** Portal area exhibiting congestion of the portal vein (P.V), distortion of the epithelial lining of the bile duct branches (D), and inflammatory cells infiltration (red arrow). **j (X1000):** Dark brown deposition inside the hepatocytes (B) is noticed**. K (X400), l (X1000):** Melamine-exposed rats co-treated with Se-NPs@starch show partial recovery that is observed in the form of moderate congestion of the central vein (CV) and less degenerative changes (chevron) of the hepatic parenchyma, particularly hepatocytes that show less ballooning and cytoplasmic vacuolization (arrow).

The microscopical examination of the renal tissues for the control group and Se-NPs@starch exposed group revealed a normal histological structure of the renal cortex; the renal corpuscle contained normal glomerular tuft with plentiful capsular space enveloped by intact Bowman's capsule in addition to intact tubular epithelial cells of both proximal and distal convoluted tubules (PCT & DCT) as illustrated in **Fig. 10a** and **10b,** respectively. While the renal tissue sections from the melamine-exposed group exhibited various histopathological alterations in the renal corpuscles, glomeruli, PCT, DCT, and renal vasculature **(Fig. 10c-g)**. Some renal corpuscles revealed widening of Bowman's capsule **(Fig. 10c-e)** and widening of capsular space **(Fig. 10c, d)**, while others showed distortion and shrinkage of Bowman's capsule **(Fig. 10f, g)** with a narrowed capsular space **(Fig. 10e).** Moreover, some renal corpuscles revealed loss of glomeruli with a decreased number (hypocellularity) of mesangial cells **(Fig. 10c),** while others showed a complete loss of cells **(Fig. 10d).** Peri-glomerular edema was also plentiful **(Fig. 10d).** Congestion of glomerular capillary tuft **(Fig. 10c-g)** and diminished glomeruli with a prominent nuclear condensation were also detectable **(Fig. 10f, g).** In addition, degeneration, and necrosis of PCT and DCT with desquamated epithelial cells were observed **(Fig. 10d-g).** Also, some parts of DCT were lined by squamous cells and possess vacuolization and desquamation of other lining cells with pyknosis **(Fig. 10d).** Severe interstitial **(Fig. 10c)** and vascular **(Fig. 10g)** congestion in addition to hyalinization **(Fig. 10f, g)** were noticed. On the other hand, the melamine-exposed group co-treated with Se-NPs@starch demonstrated a remarkable improvement in the histological architecture. The renal cortex was nearly normal with less degeneration, congestion, and hyalinization **(Fig. 10h)**.

Moreover, the sections of renal medulla obtained from the control group and Se-NPs@starch exposed group revealed a normal histological structure of collecting tubules as observed in **Fig 10i**

&10j, respectively, while vacuolar degeneration of collecting tubules, hyalinization, and congestion of interstitial blood capillaries were prominent in those obtained from the melamine-exposed group **(Fig. 10k)**. In contrast, a marked improvement of renal medulla with less degenerated collecting tubules was observed in the melamine-exposed group co-treated with Se-NPs@starch (**Fig. 10l**).

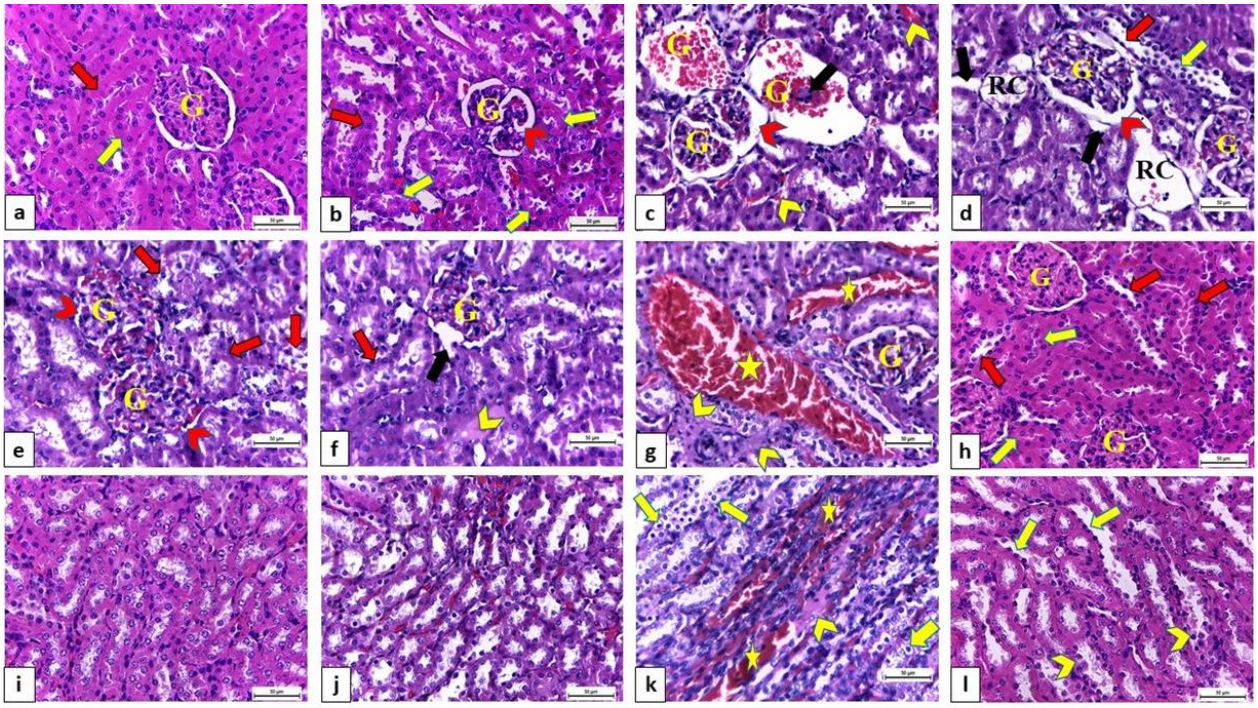

a, i: Control group; b, j: Nano-selenium group; c-g and k: Melamine group; h, l: Melamine and nano-selenium group

Fig. 10. A photomicrograph of H and E-stained sections of rats' renal tissues at X400 showing: a: The control group reveals a normal structure of the renal corpuscle containing glomerulus (G), PCT (yellow arrow), and DCT (red arrow). **b:** The Se-NPs@starch exposed group indicates normal glomerular tuft (G) with plentiful capsular space enveloped by intact Bowman's capsule (chevron), intact tubular epithelial cells of PCT (yellow arrow), and DCT (red arrow). **c-g:** The melamine-exposed group with various histopathological alterations. **c:** Some renal corpuscles present widening of capsular space (red chevron) and congestion of glomerular tuft (G) with hypocellularity of mesangial cells (black arrow). Furthermore, interstitial congestion (yellow

chevron) is observed. **d:** Some renal corpuscles (RC) demonstrating loss of glomeruli with peri-glomerular edema (black arrow), while others showing congestion of glomerulus (G) with widened capsular spaces (red chevron). Also, some degenerated DCT are lined by squamous cells (red arrow) and possess vacuolization and desquamation of other lining cells with pyknosis (yellow arrow). **e:** Some renal corpuscles show congested glomeruli (G) with narrowed capsular spaces (red chevron). Moreover, degenerated renal tubules (red arrow) were plentiful. **f:** Discontinuous Bowman's capsule (black arrow) and distorted renal corpuscle with a diminished glomerular tuft (G) are observed. Degenerated renal tubules with desquamated epithelial cells (red arrow) are also noticed in addition to hyalinization (yellow chevron). **g:** Severe vascular congestion (yellow star) and hyalinization (yellow chevron) are observed. **h:** The melamine-exposed rats co-treated with Se-NPs@starch show restoration of most renal corpuscles, glomeruli (G), and renal tubules (yellow arrow), while some renal tubules still show degeneration (red arrow). **i:** Renal medulla of the control group reveals the normal structure of collecting tubules. **j:** The Se-NPs@starch exposed group exhibits nearly normal collecting tubules of the medulla. **k:** The melamine-exposed group shows a prominent vacuolar degeneration of collecting tubules (yellow arrow), hyalinization (yellow chevron), and congestion of interstitial blood capillaries (yellow star). **l:** The melamine-exposed group co-treated with Se-NPs@starch demonstrates a partial recovery of renal medulla with less degenerated collecting tubules (yellow chevron). Also, some collecting tubules appear with squamous lining cells (yellow arrow).

Scoring criteria for the observed histopathological changes in the hepatic and renal architectures of different groups are presented in **Fig. 11**. The highest score in all histopathological parameters was noticed in the melamine-exposed group, while the SeNPs co-treated group revealed a substantial reduction in the elevated histopathological score induced by melamine.

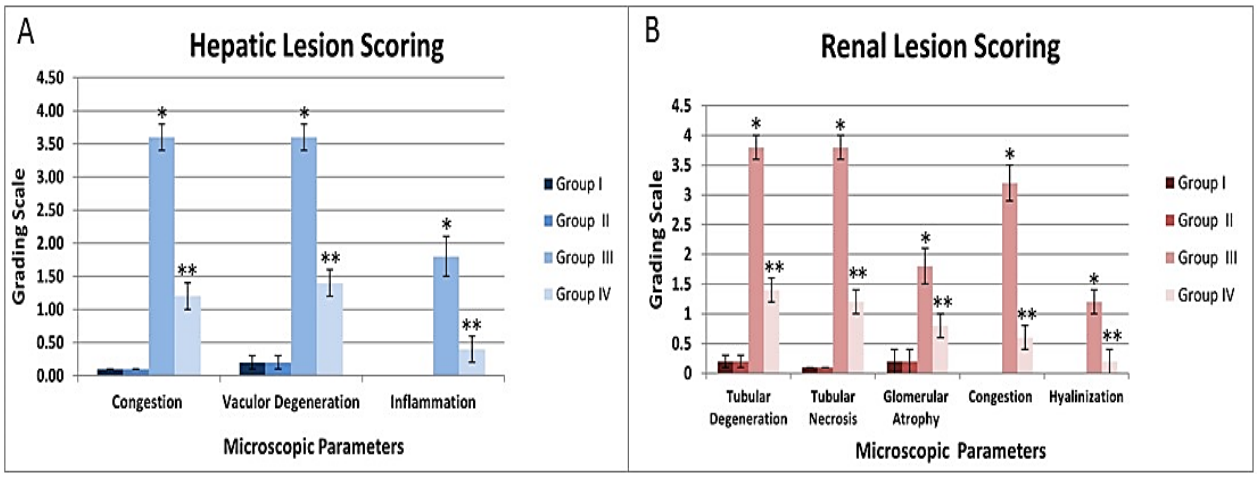

Fig. 11. Bar chart showing the microscopic lesion scoring in both liver (A) and kidney (B) sections of different groups. Scores are presented as mean values ± SEM (n= 5 slides representing 5 rats/group). *indicates statistically different from the control negative group ($p< 0.05$). ** indicates statistically different from the melamine-intoxicated group ($p< 0.05$). Note: 0= normal histology, 1= mild, 2= moderate, 3= severe, and 4= extensive severe tissue damage.

6. Immunohistochemical finding

According to our immunohistochemical findings in **Fig. 12**, liver sections obtained from both control and Se-NPs@starch exposed rats exhibited a negative reaction to caspase 3, while a strong immuno-expression was noticed in the melamine-exposed one. However, the liver sections obtained from the group exposed to melamine and co-treated with Se-NPs@starch indicated a mild expression of caspase 3 **(Fig. 12).**

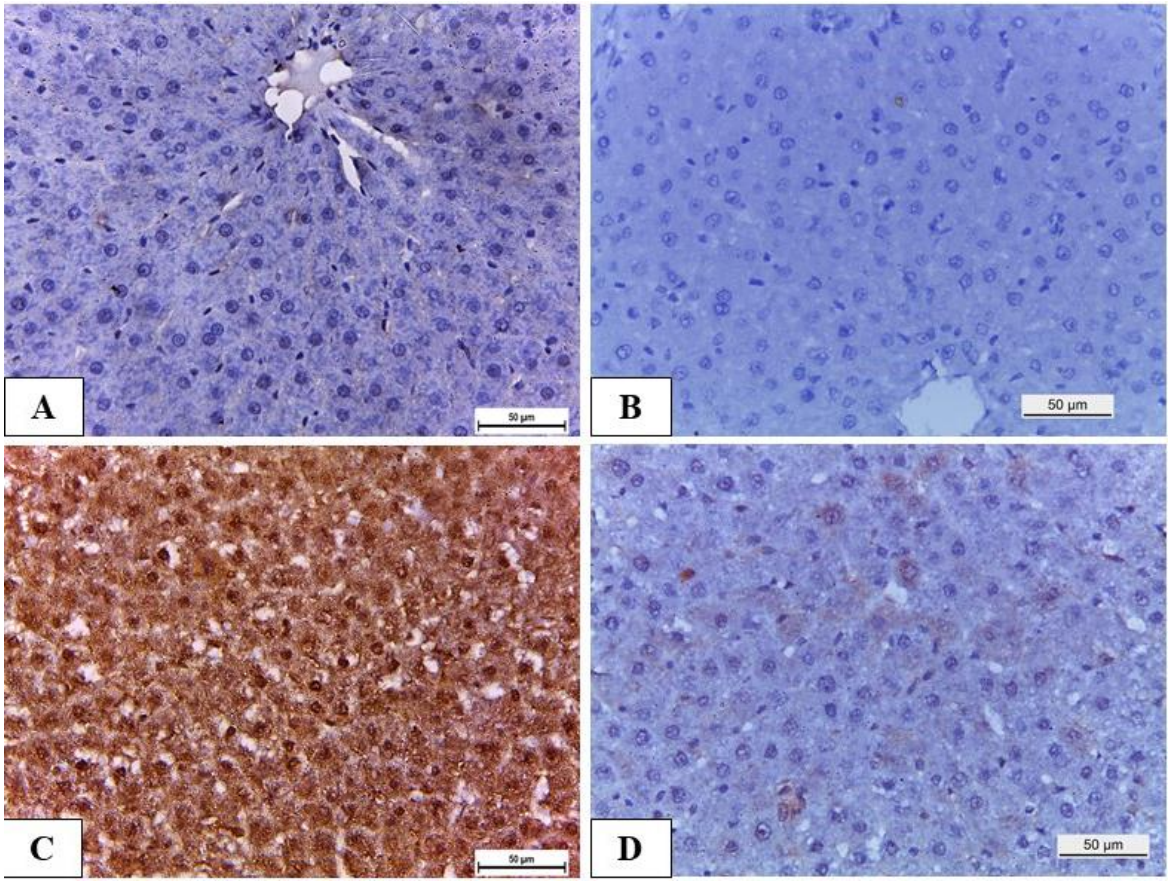

Fig. 12. A photomicrograph demonstrating immune expression in the caspase 3 stained liver sections (x400). A & B. Negative caspase expression in the hepatic tissue obtained from the control **(A)** and Se-NPs@starch treated group **(B)**. **C.** Intense expression in the melamine-exposed group. **D.** Mild expression in the melamine-exposed group co-treated with Se-NPs@starch.

Furthermore, the renal tissues of both control and Se-NPs@starch exposed groups displayed a mild positive immunoreactivity to caspase 3. In contrast, the melamine-exposed group revealed a strong positive immune reaction. However, a moderate immunoreactivity was noticed in the melamine-intoxicated group co-treated with Se-NPs@starch **(Fig. 13).**

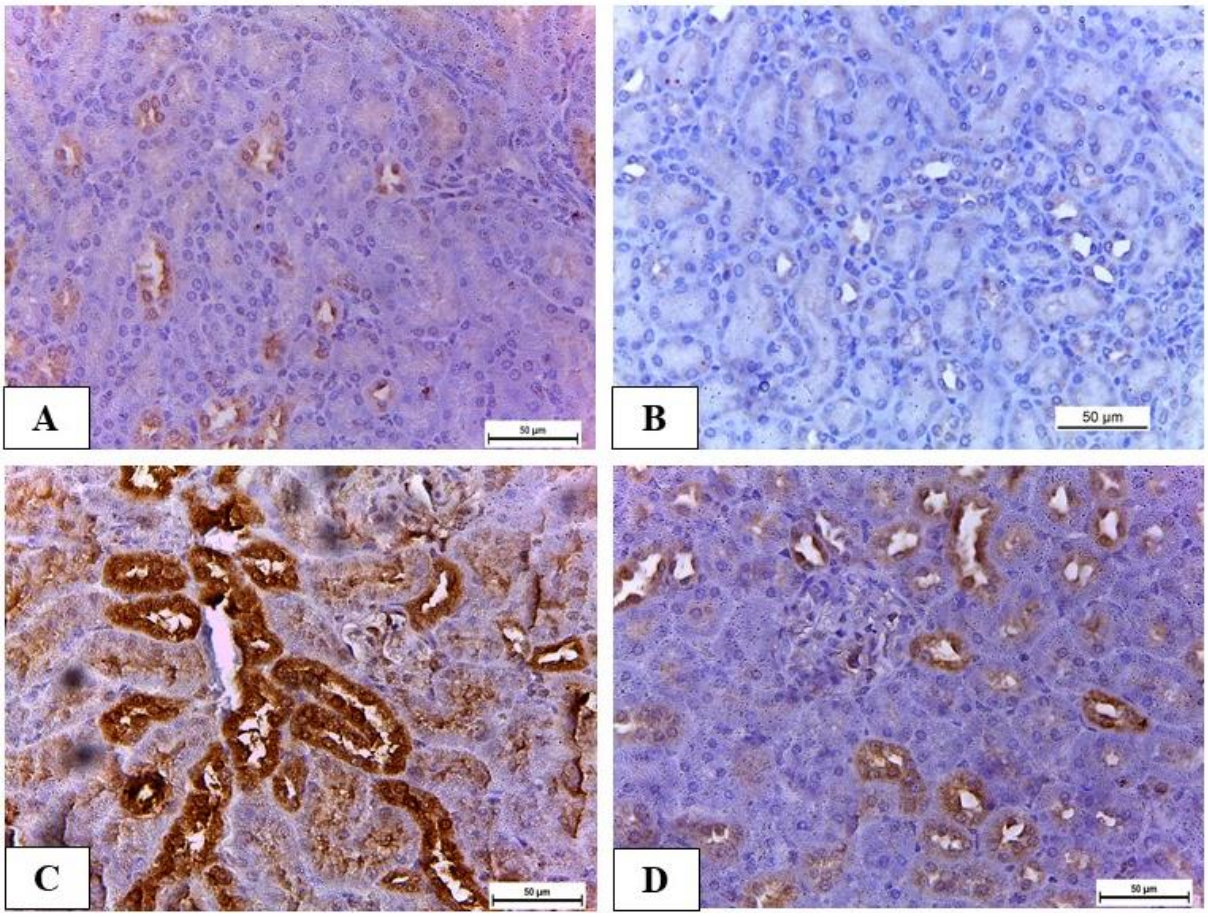

Fig. 13. A photomicrograph demonstrating caspase 3 expression in the renal tissue sections (x400). A & B. Mild positive expression in the renal tissue obtained from the control **(A)** and Se-NPs@starch exposed group **(B)**. **C.** Intense expression in the melamine-exposed group. **D.** Moderate expression in the melamine-exposed group co-treated with Se-NPs@starch.

According to the data analysis, the melamine-intoxicated group demonstrated a remarkable elevation ($p< 0.05$) in the area% covered by caspase 3 in both hepatic and renal tissues compared to the control and Se-NPs@starch exposed group. On the other hand, the concurrent administration of Se-NPs@starch significantly ($p< 0.05$) reduced the caspase 3 area% induced by melamine in both hepatic and renal tissues by 87.92% and 65.9%, respectively, compared to the melamine-intoxicated group **(Fig. 14).**

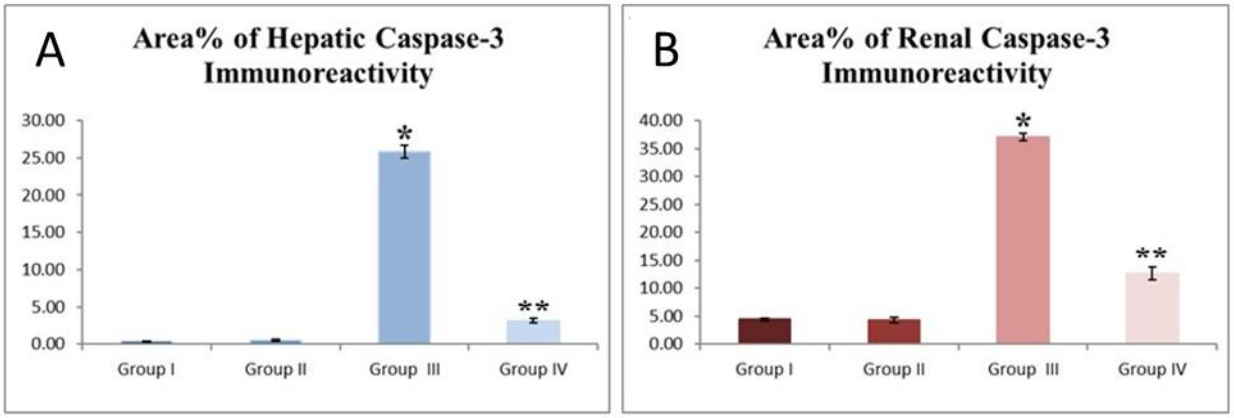

Fig. 14. Morphometrical analysis representing the protective effect of Se-NPs against the melamine-induced high area % of the hepatic (A) and renal (B) caspase 3-stained sections in rats. Data are presented as mean ± SEM (n=5 fields/group). ***** indicates statistically different from the control negative group ($p< 0.05$). ****** indicates statistically different from the melamine-intoxicated group ($p< 0.05$).

4. Discussion

The kidney is the major target organ in melamine toxicity, but there are some other tissues such as the liver, muscles, colon, and spleen that were investigated for melamine toxicity [55]. This study has been focused on testing the ability of oral administration of Se-NPs@starch to attenuate melamine-induced liver and kidney dysfunction. Therefore, the serum AST and ALT activities were assessed as the principal hallmarks of liver toxicity [56]. According to the present investigation, melamine induces severe hepatic damage as represented by markedly elevated serum functions of AST and ALT which further evidenced by severe histopathological alternations in the normal structure of hepatic tissues as shown in **Fig. 9 (d-j)** that indicated severe damage of the cellular membrane followed by leakage of hepatic enzymes into the bloodstream [57]. These results are in good agreement with those reported recently by Abd-Elhakim et al. [21]. However, treatment with Se-NPs@starch in group IV markedly decreased the serum activities of both ALT

and AST, in addition to improving liver functions, which are highly indicative of the hepatoprotective effect of Se-NPs@starch on melamine-induced hepatic impairment. These findings are consistent with Bai et al. and Sohrabi et al. [58, 59]. Additionally, the ameliorative effects of Se-NPs@starch are also confirmed by the less hepatocellular damage observed in the histopathological examination of liver tissues as shown in **Fig. 9 (k & l)**. These results are in good agreement with those reported by Amin et al., Bai et al., and Hamza et al. [58, 60, 61]. These outcomes may be attributed to maintaining the hepatocyte's integrity or regeneration of damaged hepatocytes [62]. Furthermore, urea is considered the initial acute renal biomarker that elevates by any type of renal injury. While creatinine only elevates when most of the kidney function is lost, therefore, it is considered the most reliable renal indicator [63]. Consequently, any significant elevation in the serum urea and creatinine levels can indicate kidney damage. Our results reveal that melamine-intoxicated rats exhibited a significant elevation in the serum creatinine and urea levels, indicating melamine-induced renal glomerular impairment. These findings are consistent with those of Al-Seeni et al. and Abd-Elhakim et al. [21, 64]. Moreover, the renal damage induced by melamine is indicated histopathologically by severe deterioration of renal architecture as shown in **Fig. 10 (c-g & k)** which was also observed by Lee et al. [65], Abd-Elhakim et al. [21], Lee et al. [65], Yasui et al. [66] and Peerakietkhajorn et al. [67]. In contrast, the concomitant administration of Se-NPs@starch with melamine considerably decreases the serum urea and creatinine levels. Moreover, administration of Se-NPs@starch substantially restores the melamine-induced histological alterations to the kidney tissues as observed in **Fig. 10 (h & l)** supporting the nephroprotective property of Se-NPs@starch against melamine toxicity. These results agree with those obtained by others [68, 69]. The nephroprotective efficiency role of the Se-NPs@starch

could be due to its potent action in scavenging free radicals [70], thus protect the cellular structure from oxidative damage [71].

Based on the obtained findings, oxidative stress and apoptosis are involved in the pathophysiology of the hepato-renal toxicity induced by melamine. Here, the levels of lipid peroxidation marker and GSH, in addition to mRNA expression level for GPx and Nrf2 were assessed to evaluate the level of oxidative stress. Compared to the control, the MDA level in both tissue homogenates was strongly elevated, while the content of GSH and the mRNA expression level for GPx was sharply reduced in the melamine-intoxicated rats. Therefore, our results suggest that melamine elevates the susceptibility of tissue to oxidative damage via increasing oxidative stress and reduction of endogenous antioxidant capacity in both tissues. Our findings coincide with the previous results stated by Al-Seeni et al. and Abd-Elhakim et al. [21, 64].

A marked elevation of MDA concentration reflected the severity of cell damage resulted from the oxidation of unsaturated fatty acids. Moreover, a significant depletion in antioxidant enzymes (GPx and GSH) reflects the impaired antioxidant defense mechanism to counteract the elevated levels of free radicals [72]. The molecular mechanism underlying the hepato-renal damage induced by melamine is not entirely clear. According to our results, melamine administration induced hepato-renal oxidative damage as substantiated by marked downregulation for Nrf2 mRNA gene expression. As known, Nrf2 is a key transcription factor that has a critical contributor role to protect cells from damage induced by inflammation and oxidative stress. Translocation of Nrf2, from the cytoplasm to the nucleus, was necessary for its regulation of antioxidant/detoxification enzyme expression [73]. As observed in our study, melamine downregulates the Nrf2 mRNA level. This is an indicator of an oxidative stress response. On the other hand, Se-NPs@starch co-

administered group (group IV) significantly reduced the level of MDA, stabilized nonenzymatic antioxidant GSH level, and up-regulated antioxidant enzyme (GPx) mRNA expression level in the liver and kidneys. Thus, these findings suggest an ameliorating effect of Se-NPs@starch against melamine-induced excessive production of ROS. Se-NPs@starch administration results in antioxidative and nephron-protective effects as was reported by Khater et al. [69]. Furthermore, the antioxidant activity of Se-NPs@starch was reported by Bai et al. and Sheiha et al. [58, 74] for liver tissue and these findings support our results. Moreover, selenium can combat oxidative stress, consequently leading to the cellular redox balance, due to its incorporation as selenocysteine into GPx and thioredoxin reductase [74]. Se-NPs@starch lead to an increase in the activities of both GPx and glutathione S-transferase, resulting in less oxidative stress [30, 69]. In addition, Se-NPs@starch detoxify hydroperoxidase and lipid peroxides that accumulate in the cytoplasm and mitochondria. Moreover, Se improves the antioxidant enzyme capacity, thereby leading to cellular protection from oxidative damage [75]. Khalaf et al. and Rashad et al. [37, 76] verified the antioxidant effect of Se-NPs@starch. Furthermore, most recent studies link the potent antioxidant effects of Se with the activation of the Nrf2 factor. Se can upregulate the transcription of Nrf2 against metal intoxication [77], as observed in our result. The elevated levels of oxidative stress may hinder the pathway of Nrf2 and thereby enhancing the deleterious effects induced by toxic agents [78]. Zhang et al. reported that selenium triggered the Nrf2 activation and thereby upregulating the transcription of many genes like glutathione S-transferase [79]. Concerning cell death, a series of physiological symptoms is initiated as a result of several biochemical lesions induced by the rapid reaction of free radicals with cellular elements that eventually lead to apoptosis. Therefore, our study strongly recommends using Se-NPs@starch as a potent antioxidant to diminish the apoptosis induced by melamine intoxication in both hepatic and renal tissues. In

the current study, intoxication with melamine significantly induces overexpression of the mRNA expression level of both apoptotic genes; caspase-3 and c-Myc. This observation is in harmony with that of Hsieh et al. [80]. This is confirmed by a significant strong positive caspase 3 immunoreactivities of hepato-renal tissues in melamine-intoxicated rats as presented in **Fig. 12-14**. Activation of caspase 3 can be triggered either by extrinsic or intrinsic factors inducing mitochondrial stress, and it plays important role in cell apoptosis [81]. Activation of caspase 3 is an important hallmark of DNA fragmentation and nuclear condensation in apoptotic cells [68, 82]. c-Myc is a potent transcription factor that regulates the proliferation, growth, and differentiation of cells, whereas deregulation of c-Myc as in the situation of cellular stress induces apoptosis [83] and suggested that Bax and caspase activation are involved in c-Myc induced apoptosis. The hepato-renal cell death induced by melamine may be attributed to the excessive release of ROS after mitochondrial dysfunction. Yiu et al. reported that melamine activates Ca2-sensing receptors which in turn causes a sustained Ca2 entry in the cell [84]. Cell death may be mediated either by ROS generation together with elevation of Ca ions inducing a caspase-mediated apoptotic pathway or through activation of the mitochondrial proapoptotic (Bax-1/ Bcl-2) pathway and ROS-mediated cytotoxicity [55]. Therefore, the potent anti-apoptotic activity of affordable Se-NPs@starch has been commonly postulated as one of the vital mechanisms underlying its beneficial bioactive properties. This activity was previously reported [85]. Many studies have shown the potential ameliorative effect of Se-NPs@starch against oxidative stress, nuclear damage, and cell death [76, 85] that may be due to the ability of Se-NPs@starch to enhance the antioxidant defense mechanism, scavenge free radicals efficiently [86], upregulate Nrf2 and heme oxygenase-1, as well as impede the inflammatory response and apoptotic cascade [85].

5. Conclusions

A versatile and green method for the fabrication of Se-NPs that are effectively stabilized by starch is described. The starch-stabilized Se-NPs were characterized by XPS, FT-IR, EDS elemental mapping, and TEM investigations. Se-NPs are distributed homogeneously over the starch surface and have a spherical shape with a particle size ranging from 20 to 140 nm. The protective efficacy of starch stabilized Se-NPs on the melamine-induced hepato-renal toxicity has been evaluated. Melamine ingestion can result in a range of toxicological effects on the liver and kidneys. The intoxication with melamine is characterized by an elevation of ALT, AST, serum urea, and creatinine, besides *higher MDA* levels, an increase in the expression level of the apoptosis-related gene, a reduction in the GSH, and a decrease in the expression level of antioxidant genes. These findings were associated with a strong positive immune expression of caspase-3 as well as severe distortion and alteration in the hepato-renal tissues. Fascinatingly, the daily oral administration of starch-stabilized Se-NPs (2 mg Se-NPs@starch/kg/day) for 28 days significantly reduces the apoptotic effect produced by melamine intoxication (300 mg melamine/kg/day) in the liver and kidney tissues of adult rats. Moreover, Se-NPs@starch can substantially improve the liver and kidney function parameters, alleviate the oxidative stress, apoptosis, and histopathological injuries exerted by melamine. This study highlights the detrimental effects of melamine ingestion on the liver and kidneys and provides Se-NPs stabilized by starch as an affordable and effective material to inhibit these toxic effects.

Funding

This study received no support from public, private, or non-profit funding agencies.

Data Availability

Not applicable

Conflict of interest

The authors declare no known competing interests.

Author contributions

All authors conceived the study and designed the experimental protocol. Drweesh E.A., Abou-El-Sherbini K.S., Elzahany E.A.M., and Elnagar M.M. prepared and described the X-ray photoelectron spectroscopy (XPS), Fourier-transform infrared (FTIR), and transmission electron microscope (TEM) observations for the produced Se-NPs in comparison with the stabilizing agent and embedding host (starch). Ahmed Z.S.O. and Yasin N.A.E. performed the histopathological and immunohistochemical investigations and drafted the manuscript. Galal M.K. performed the biochemical and molecular assays. All authors read, revised, and approved the final manuscript.

Ethical Approval

Rats were treated humanely according to NIH guidelines, and the experimental procedure was accepted by the Institutional Animal Care and Use Committee (IACUC) of the Faculty of Veterinary Medicine, Cairo University (Approval number Vet CU28042021291).

References

[1] A.K.-c. Hau, T.H. Kwan, P.K.-t. Li, Melamine Toxicity and the Kidney, J. Am. Soc. Nephrol. 20 (2009) 245. https://doi.org/10.1681/asn.2008101065.

[2] J.L. Dorne, D.R. Doerge, M. Vandenbroeck, J. Fink-Gremmels, W. Mennes, H.K. Knutsen, F. Vernazza, L. Castle, L. Edler, D. Benford, Recent advances in the risk assessment of melamine and cyanuric acid in animal feed, Toxicol. Appl. Pharmacol. 270 (2013) 218-229. https://doi.org/10.1016/j.taap.2012.01.012.

[3] E.P.o.C.i.t.F. Chain, E. EFSA Panel on Food Contact Materials, Flavourings, P. Aids, Scientific Opinion on Melamine in Food and Feed, EFSA J. 8 (2010) 1573. https://doi.org/10.2903/j.efsa.2010.1573.

[4] A.L. Bolden, J.R. Rochester, C.F. Kwiatkowski, Melamine, beyond the kidney: A ubiquitous endocrine disruptor and neurotoxicant?, Toxicol. Let. 280 (2017) 181-189. https://doi.org/10.1016/j.toxlet.2017.07.893.

[5] R.L.M. Dobson, S. Motlagh, M. Quijano, R.T. Cambron, T.R. Baker, A.M. Pullen, B.T. Regg, A.S. Bigalow-Kern, T. Vennard, A. Fix, R. Reimschuessel, G. Overmann, Y. Shan, G.P. Daston, Identification and Characterization of Toxicity of Contaminants in Pet Food Leading to an Outbreak of Renal Toxicity in Cats and Dogs, Toxicol. Sci. 106 (2008) 251-262. https://doi.org/10.1093/toxsci/kfn160.

[6] C.-Y. Chien, C.-F. Wu, C.-C. Liu, B.-H. Chen, S.-P. Huang, Y.-H. Chou, A.-W. Chang, H.-H. Lee, C.-H. Pan, W.-J. Wu, J.-T. Shen, M.-Y. Chang, C.-H. Huang, J. Shiea, T.-J. Hsieh, M.-T. Wu,

High melamine migration in daily-use melamine-made tableware, J. Hazard. Mater. 188 (2011) 350-356. https://doi.org/10.1016/j.jhazmat.2011.01.128.

[7] V. Bhalla, P.C. Grimm, G.M. Chertow, A.C. Pao, Melamine nephrotoxicity: an emerging epidemic in an era of globalization, Kidney Int. 75 (2009) 774-779. https://doi.org/10.1038/ki.2009.16.

[8] Z. Wang, H. Luo, W. Tu, H. Yang, W.H. Wong, W.T. Wong, K.F. Yung, N. Zhou, J. Zhang, X. Li, W. Guo, D. Mu, F. Li, M. Mao, Y.L. Lau, Melamine-tainted milk product-associated urinary stones in children, Pediatr. Int. 53 (2011) 489-496. https://doi.org/10.1111/j.1442-200X.2010.03284.x

[9] B. Puschner, R.H. Poppenga, L.J. Lowenstine, M.S. Filigenzi, P.A. Pesavento, Assessment of melamine and cyanuric acid toxicity in cats, J. Vet. Diagn. Invest. 19 (2007) 616-24. https://doi.org/10.1177/104063870701900602.

[10] M.E. Thompson, M.R. Lewin-Smith, V.F. Kalasinsky, K.M. Pizzolato, M.L. Fleetwood, M.R. McElhaney, T.O. Johnson, Characterization of melamine-containing and calcium oxalate crystals in three dogs with suspected pet food-induced nephrotoxicosis, Vet. Pathol. 45 (2008) 417-26. https://doi.org/10.1354/vp.45-3-417.

[11] J.Y. Yhee, C.A. Brown, C.H. Yu, J.H. Kim, R. Poppenga, J.H. Sur, Retrospective study of melamine/cyanuric acid-induced renal failure in dogs in Korea between 2003 and 2004, Vet. Pathol .46 (2009) 348-54. https://doi.org/10.1354/vp.46-2-348.

[12] Y. Wang, F. Liu, Y. Wei, D. Liu, The effect of exogenous melamine on rat hippocampal neurons, Toxicol. Ind. Health. 27 (2011) 571-6. https://doi.org/10.1177/0748233710395347.

[13] C.Y. Chu, K.O. Chu, J.Y.W. Chan, X.Z. Liu, C.S. Ho, C.K. Wong, C.M. Lau, T.L. Ting, T.F. Fok, K.P. Fung, C.C. Wang, Distribution of melamine in rat foetuses and neonates, Toxicol. Lett. 199 (2010) 398-402. https://doi.org/10.1016/j.toxlet.2010.10.004.

[14] Q.-x. Zhang, G.-y. Yang, J.-t. Li, W.-x. Li, B. Zhang, W. Zhu, Melamine induces sperm DNA damage and abnormality, but not genetic toxicity, Regul. Toxicol. Pharmacol. 60(1) (2011) 144-150. https://doi.org/10.1016/j.yrtph.2011.03.004.

[15] Y. Lv, Z. Liu, Y. Tian, H. Chen, Effect on morphology, oxidative stress and energy metabolism enzymes in the testes of mice after a 13-week oral administration of melamine and cyanuric acid combination, Regul. Toxicol. Pharmacol. 65 (2013) 183-188. https://doi.org/10.1016/j.yrtph.2012.11.011.

[16] S. Khan, T. Ahmad, C.V. Parekh, P.P. Trivedi, S. Kushwaha, G. Jena, Investigation on sodium valproate induced germ cell damage, oxidative stress and genotoxicity in male Swiss mice, Reproductive Toxicology 32 (2011) 385 394. https://doi.org/10.1016/j.reprotox.2011.09.007.

[17] F.Q. Schafer, G.R. Buettner, Redox environment of the cell as viewed through the redox state of the glutathione disulfide/glutathione couple, Free Radic. Biol. Med. 30(11) (2001) 1191-1212. https://doi.org/10.1016/S0891-5849(01)00480-4.

[18] M. Moshahid Khan, S.S. Raza, H. Javed, A. Ahmad, A. Khan, F. Islam, M.M. Safhi, F. Islam, Rutin Protects Dopaminergic Neurons from Oxidative Stress in an Animal Model of Parkinson's Disease, Neurotox. Res. 22 (2012) 1-15. https://doi.org/10.1007/s12640-011-9295-2.

[19] M. Gałażyn-Sidorczuk, M.M. Brzóska, M. Jurczuk, J. Moniuszko-Jakoniuk, Oxidative damage to proteins and DNA in rats exposed to cadmium and/or ethanol, Chem. Biol. Interact. 180 (2009) 31-38. https://doi.org/10.1016/j.cbi.2009.01.014.

[20] A.F. Hamouda, A.A.E. Amin, S.S. Ibrahim, M.A. Mahmoud, Potential Ameliorative Effect of Bee Honey on Experimentally Induced Melamine Formaldehyde Toxicity in Male Rats, World Vet. J. 9 (2019) 146-157. https://dx.doi.org/10.36380/scil.2019.wvj19.

[21] Y.M. Abd-Elhakim, W.A.M. Mohamed, K.M. El.Bohi, H.A. Ali, F.A. Mahmoud, T.M. Saber, Prevention of melamine-induced hepatorenal impairment by an ethanolic extract of Moringa oleifera: Changes in KIM-1, TIMP-1, oxidative stress, apoptosis, and inflammation-related genes, Gene 764 (2021) 145083. https://doi.org/10.1016/j.gene.2020.145083.

[22] V. Vijayakumar, S.K. Samal, S. Mohanty, S.K. Nayak, Recent advancements in biopolymer and metal nanoparticle-based materials in diabetic wound healing management, Int. J. Biol. Macromol. 122 (2019) 137-148. https://doi.org/10.1016/j.ijbiomac.2018.10.120.

[23] K. Saravanakumar, B. Sriram, A. Sathiyaseelan, A.V.A. Mariadoss, X. Hu, K.-S. Han, V. Vishnupriya, D. MubarakAli, M.-H. Wang, Synthesis, characterization, and cytotoxicity of starch-encapsulated biogenic silver nanoparticle and its improved anti-bacterial activity, Int. J. Biol. Macromol. 182 (2021) 1409-1418. https://doi.org/10.1016/j.ijbiomac.2021.05.036.

[24] C. Jensen, J. Pallauf, Estimation of the selenium requirement of growing guinea pigs (Cavia porcellus), J. Anim. Physiol. Anim. Nutr. 92 (2008) 481-491. https://doi.org/10.1111/j.1439-0396.2007.00738.x.

[25] W. Li, M. Guo, Y. Liu, W. Mu, G. Deng, C. Li, C. Qiu, Selenium induces an anti-tumor effect via inhibiting intratumoral angiogenesis in a mouse model of transplanted canine mammary tumor cells, Biol. Trace Elem. Res. 171 (2016) 371-379.https://doi.org/10.1007/s12011-015-0554-6.

[26] L. He, J. Zhao, L. Wang, Q. Liu, Y. Fan, B. Li, Y.-L. Yu, C. Chen, Y.-F. Li, Using nano-selenium to combat Coronavirus Disease 2019 (COVID-19)?, Nano Today 36 (2021) 101037. https://doi.org/10.1016/j.nantod.2020.101037.

[27] Y.-C. Chen, K.S. Prabhu, A. Das, A.M. Mastro, Dietary selenium supplementation modifies breast tumor growth and metastasis, Int. J. Cancer Res. 133 (2013) 2054-2064. https://doi.org/10.1002/ijc.28224.

[28] D. Sun, Y. Liu, Q. Yu, X. Qin, L. Yang, Y. Zhou, L. Chen, J. Liu, Inhibition of tumor growth and vasculature and fluorescence imaging using functionalized ruthenium-thiol protected selenium nanoparticles, Biomaterials 35 (2014) 1572-1583. https://doi.org/10.1016/j.biomaterials.2013.11.007.

[29] N. Filipović, D. Ušjak, M.T. Milenković, K. Zheng, L. Liverani, A.R. Boccaccini, M.M. Stevanović, Comparative Study of the Antimicrobial Activity of Selenium Nanoparticles With Different Surface Front. Bioeng. Biotechnol. 8 (2021) 624621. https://doi.org/10.3389/fbioe.2020.624621.

[30] D. Peng, J. Zhang, Q. Liu, E.W. Taylor, Size effect of elemental selenium nanoparticles (Nano-Se) at supranutritional levels on selenium accumulation and glutathione S-transferase activity, J. Inorg. Biochem. 101 (2007) 1457-1463. https://doi.org/10.1016/j.jinorgbio.2007.06.021.

[31] H. Wang, J. Zhang, H. Yu, Elemental selenium at nano size possesses lower toxicity without compromising the fundamental effect on selenoenzymes: Comparison with selenomethionine in mice, Free Radical Biology and Medicine 42 (2007) 1524-1533. https://doi.org/10.1016/j.freeradbiomed.2007.02.013.

[32] J.-S. Zhang, X.-Y. Gao, L.-D. Zhang, Y.-P. Bao, Biological effects of a nano red elemental selenium, Biofactors 15 (2001) 27-38.

[33] C. Pelyhe, M. Mézes, Myths and facts about the effects of nano selenium in farm animals–mini-review, Eur. Chem. Bull. 2(12) (2013) 1049-1052.

[34] Y. Wang, X. Yan, L. Fu, Effect of selenium nanoparticles with different sizes in primary cultured intestinal epithelial cells of crucian carp, Carassius auratus gibelio, Int. J. Nanomedicine 8 (2013) 4007-4013. https://doi.org/10.2147/IJN.S43691.

[35] K.S. Abou-El-Sherbini, M.H.A. Amer, M.S. Abdel-Aziz, E.M.A. Hamzawy, W. Sharmoukh, M.M. Elnagar, Encapsulation of Biosynthesized Nanosilver in Silica Composites for Sustainable Antimicrobial Functionality, Global Challenges 2 (2018) 1800048. https://doi.org/10.1002/gch2.201800048.

[36] Y.M. Abd El-Hakim, A. Abdel-Rahman Mohamed, S.I. Khater, A. Hamed Arisha, M.M.M. Metwally, M.A. Nassan, M.E. Hassan, Chitosan-Stabilized Selenium Nanoparticles and Metformin Synergistically Rescue Testicular Oxidative Damage and Steroidogenesis-Related Genes Dysregulation in High-Fat Diet/Streptozotocin-Induced Diabetic Rats, Antioxidants 10 (2021) 17.

[37] M.M. Rashad, M.K. Galal, K.S. Abou-El-Sherbini, A.M. El-Behairy, E.M. Gouda, S.Z. Moussa, Nano-sized selenium attenuates the developmental testicular toxicity induced by di-n-butyl phthalate in pre-pubertal male rats, Biomed. Pharmacother. 107 (2018) 1754-1762. https://doi.org/10.1016/j.biopha.2018.09.006.

[38] D.W. Bashir, M.M. Rashad, Y.H. Ahmed, E.A. Drweesh, E.A.M. Elzahany, K.S. Abou-El-Sherbini, E.M.M. El-Leithy, The ameliorative effect of nanoselenium on histopathological and biochemical alterations induced by melamine toxicity on the brain of adult male albino rats, Neurotoxicology 86 (2021) 37-51.https://doi.org/10.1016/j.neuro.2021.06.006.

[39] C.K. Senthil kumaran, S. Agilan, D. Velauthapillai, N. Muthukumarasamy, M. Thambidurai, T.S. Senthil, R. Balasundaraprabhu, Synthesis and Characterization of Selenium Nanowires, ISRN Nanotechnology 2011 (2011) 589073.https://doi.org/10.5402/2011/589073.

[40] M.A. Rezvanfar, M.A. Rezvanfar, A.R. Shahverdi, A. Ahmadi, M. Baeeri, A. Mohammadirad, M. Abdollahi, Protection of cisplatin-induced spermatotoxicity, DNA damage and chromatin abnormality by selenium nano-particles, Toxicol. Appl. Pharmacol. 266 (2013) 356-365. https://doi.org/10.1016/j.taap.2012.11.025.

[41] L. An, J. Fu, T. Zhang, Reversible effects of vitamins C and E combination on cognitive deficits and oxidative stress in the hippocampus of melamine-exposed rats, Pharmacol. Biochem. Behav. 132 (2015) 152-159. https://doi.org/10.1016/j.pbb.2015.03.009.

[42] G.L. Ellman, Tissue sulfhydryl groups, Arch. Biochem. Biophys. 82 (1959) 70-77. https://doi.org/10.1016/0003-9861(59)90090-6

[43] H. Ohkawa, N. Ohishi, K. Yagi, Assay for lipid peroxides in animal tissues by thiobarbituric acid reaction, Anal. Biochem. 95 (1979) 351-358. https://doi.org/10.1016/0003-2697(79)90738-3.

[44] M.M. Bradford, A rapid and sensitive method for the quantitation of microgram quantities of protein utilizing the principle of protein-dye binding, Anal. Biochem. 72 (1976) 248-254.https://doi.org/10.1016/0003-2697(76)90527-3.

[45] K.J. Livak, T.D. Schmittgen, Analysis of Relative Gene Expression Data Using Real-Time Quantitative PCR and the 2−ΔΔCT Method, Methods 25 (2001) 402-408.https://doi.org/10.1006/meth.2001.1262.

[46] J.D. Bancroft, M. Gamble, Theory and practice of histological techniques, 6th ed. , Churchill Livingstone/Elsevier health sciences, Philadelphia, PA., 2008.

[47] A.A.A. Khalaf, M.A. Elhady, E.I. Hassanen, A.A. Azouz, M.A. Ibrahim, M.K. Galal, P.A. Noshy, R.A. Azouz, Antioxidant Role of Carvacrol Against Hepatotoxicity and Nephrotoxicity Induced by Propiconazole in Rev. bras. farmacogn. 31 (2021) 67-74.10.1007/s43450-021-00127-8.

[48] S. Nath, S.K. Ghosh, S. Panigahi, T. Thundat, T. Pal, Synthesis of selenium nanoparticle and its photocatalytic application for decolorization of methylene blue under UV irradiation, Langmuir 20 (2004) 7880-7883. https://doi.org/10.1021/la049318l.

[49] Å. Rindlav-Westling, P. Gatenholm, Surface Composition and Morphology of Starch, Amylose, and Amylopectin Films, Biomacromolecules 4 (2003) 166-172. https://doi.org/10.1021/bm0256810.

[50] M. Kazemi, A. Akbari, Z. Sabouri, S. Soleimanpour, H. Zarrinfar, M. Khatami, M. Darroudi, Green synthesis of colloidal selenium nanoparticles in starch solutions and investigation of their photocatalytic, antimicrobial, and cytotoxicity effects, Bioprocess Biosyst. Eng 44 (2021) 1215-1225. https://doi.org/10.1007/s00449-021-02515-9.

[51] J. M. Andrews, Determination of minimum inhibitory concentrations, J. Antimicrob. Chemother. 48 (2001) 5-16.

[52] S. S. Salem, M. M.G. Fouda, A. Fouda, M. A. Awad, E. M. Al-Olayan, A. A. Allam, T.I. Shaheen, Antibacterial, Cytotoxicity and Larvicidal Activity of Green Synthesized Selenium Nanoparticles Using Penicillium corylophilum, J. Clust. Sci. 32 (2021) 351-361. https://doi.org/10.1007/s10876-020-01794-8.

[53] M. Abu-Elghait, M. Hasanin, A. H. Hashem, S. S. Salem, Ecofriendly novel synthesis of tertiary composite based on cellulose and myco-synthesized selenium nanoparticles: Characterization, antibiofilm and biocompatibility, Int. J. Biol. Macromol. 175 (2021) 294-303. https://doi.org/10.1016/j.ijbiomac.2021.02.040.

[54] P.K. Gautam, S. Kumar, M.S. Tomar, R.K. Singh, A. Acharya, B. Ram, Selenium nanoparticles induce suppressed function of tumor associated macrophages and inhibit Dalton's lymphoma proliferation, Biochem. Biophys. Rep. 12 (2017) 172-184. https://doi.org/10.1016/j.bbrep.2017.09.005.

[55] A. Melekoğlu, H. Ekici, A. Esra, S. Karahan, Evaluation of melamine and cyanuric acid cytotoxicity: an in vitro study on L929 fibroblasts and CHO cell line, Ankara Üniversitesi Veteriner Fakültesi Dergisi 67 (2020) 399-406. https://doi.org/10.33988/auvfd.664059.

[56] Y.M. Abd-Elhakim, G.G. Moustafa, M.M. Hashem, H.A. Ali, K. Abo-El-Sooud, A.E. El-Metwally, Influence of the long-term exposure to tartrazine and chlorophyll on the fibrogenic signalling pathway in liver and kidney of rats: the expression patterns of collagen 1-α, TGFβ-1, fibronectin, and caspase-3 genes, Environ. Sci. Pollut. Res. 26 (2019) 12368-12378.https://doi.org/10.1007/s11356-019-04734-w.

[57] Q.K. Alabi, R.O. Akomolafe, O.S. Olukiran, W.J. Adeyemi, A.O. Nafiu, M.A. Adefisayo, J.G. Omole, D.I. Kajewole, O.O. Odujoko, The Garcinia kola biflavonoid kolaviron attenuates experimental hepatotoxicity induced by diclofenac, Pathophysiology 24 (2017) 281-290. https://doi.org/10.1016/j.pathophys.2017.07.003.

[58] K. Bai, B. Hong, J. He, W. Huang, Antioxidant Capacity and Hepatoprotective Role of Chitosan-Stabilized Selenium Nanoparticles in Concanavalin A-Induced Liver Injury in Mice, Nutrients 12 (2020).https://doi.org/10.3390/nu12030857.

[59] A. Sohrabi, A.A. Tehrani, S. Asri-Rezaei, A. Zeinali, M. Norouzi, Histopathological assessment of protective effects of selenium nanoparticles on rat hepatocytes exposed to Gamma radiation, Vet. Res. Forum 11 (2020) 347-353.https://doi.org/10.30466/vrf.2018.93499.2260.

[60] K.A. Amin, K.S. Hashem, F.S. Alshehri, S.T. Awad, M.S. Hassan, Antioxidant and hepatoprotective efficiency of selenium nanoparticles against acetaminophen-induced hepatic damage, Biol. Trace Elem. Res. 175 (2017) 136-145. https://doi.org/10.1007/s12011-016-0748-6.

[61] R.Z. Hamza, S.M. EL-Megharbel, T. Altalhi, A.A. Gobouri, A.A. Alrogi, Hypolipidemic and hepatoprotective synergistic effects of selenium nanoparticles and vitamin. E against acrylamide-induced hepatic alterations in male albino mice, Appl. Organomet. Chem. 34 (2020) e5458. https://doi.org/10.1002/aoc.5458.

[62] K. Patrick-Iwuanyanwu, M. Wegwu, E. Ayalogu, Prevention of CCI4-induced liver damage by ginger, garlic and vitamin E, Pak. J. Biol. Sci. 10 (2007) 617-21. https://doi.org/10.3923/pjbs.2007.617.621.

[63] L.P. Borges, V.C. Borges, A.V. Moro, C.W. Nogueira, J.B.T. Rocha, G. Zeni, Protective effect of diphenyl diselenide on acute liver damage induced by 2-nitropropane in rats, Toxicology 210 (2005) 1-8. https://doi.org/10.1016/j.tox.2005.01.002.

[64] M.N. Al-Seeni, H.A. El Rabey, S.M. Al-Solamy, The protective role of bee honey against the toxic effect of melamine in the male rat kidney, Toxicol. Ind. Health 31(2015) 485-93.https://doi.org/10.1177/0748233714551765.

[65] I.-C. Lee, S.-H. Kim, H.-S. Baek, S.-S. Kang, J.-C. Kim, Synergistic effect of melamine in combination with cyanuric acid on urinary tract toxicity in rats, J. Biomed. Res. 14 (2013) 145-153.

[66] T. Yasui, T. Kobayashi, A. Okada, S. Hamamoto, M. Hirose, K. Mizuno, Y. Kubota, Y. Umemoto, N. Kawai, K. Tozawa, B. Gao, K. Kohri, Long-term follow-up of nephrotoxicity in rats administered both melamine and cyanuric acid, BMC Res. Notes 7 (2014) 87.https://doi.org/10.1186/1756-0500-7-87.

[67] S. Peerakietkhajorn, N. Huipao, S. Hiranyachattada, Effects of Melamine and Cyanuric Acid on Renal Function and Structure in Rats, Sains Malays. 48 (2019) 1721-1728. http://dx.doi.org/10.17576/jsm-2019-4808-18.

[68] G. Albasher, S. Al Kahtani, M.S. Alwahibi, R. Almeer, Effect of Moringa oleifera Lam. methanolic extract on lead-induced oxidative stress-mediated hepatic damage and inflammation in rats, Environ. Sci. Pollut. Res. 27 (2020) 19877-19887. https://doi.org/10.1007/s11356-020-08525-6.

[69] S.I. Khater, I. Ali, A. Ahmed, Preparation and Characterization of Chitosan-Stabilized Selenium Nanoparticles for Ameliorating Experimentally Induced Diabetic Nephropathy in Rats, Arab J. Nucl. Sci. Appl. 53 (2020) 140-148. https://doi.org/10.21608/ajnsa.2020.19809.1300.

[70] M. Navarro-Alarcon, C. Cabrera-Vique, Selenium in food and the human body: A review, Sci. Total Environ. 400 (2008) 115-141. https://doi.org/10.1016/j.scitotenv.2008.06.024.

[71] A. Khurana, S. Tekula, M.A. Saifi, P. Venkatesh, C. Godugu, Therapeutic applications of selenium nanoparticles, Biomed. Pharmacother. 111 (2019) 802-812. https://doi.org/10.1016/j.biopha.2018.12.146.

[72] L.-J. Su, J.-H. Zhang, H. Gomez, R. Murugan, X. Hong, D. Xu, F. Jiang, Z.-Y. Peng, Reactive Oxygen Species-Induced Lipid Peroxidation in Apoptosis, Autophagy, and Ferroptosis, Oxid. Med. Cell. Longev. 2019 (2019) 5080843. https://doi.org/10.1155/2019/5080843.

[73] N.K. Mondal, H. Saha, B. Mukherjee, N. Tyagi, M.R. Ray, Inflammation, oxidative stress, and higher expression levels of Nrf2 and NQO1 proteins in the airways of women chronically exposed to biomass fuel smoke, Mol. Cell. Biochem. 447 (2018) 63-76. https://doi.org/10.1007/s11010-018-3293-0.

[74] A.M. Sheiha, S.A. Abdelnour, M.E. Abd El-Hack, A.F. Khafaga, K.A. Metwally, J.S. Ajarem, S.N. Maodaa, A.A. Allam, M.T. El-Saadony, Effects of Dietary Biological or Chemical-Synthesized Nano-Selenium Supplementation on Growing Rabbits Exposed to Thermal Stress, Animals 10 (2020) 430.

[75] Z. Xu, Z. Wang, J.-j. Li, C. Chen, P.-c. Zhang, L. Dong, J.-h. Chen, Q. Chen, X.-t. Zhang, Z.-l. Wang, Protective effects of selenium on oxidative damage and oxidative stress related gene expression in rat liver under chronic poisoning of arsenic, Food Chem. Toxicol. 58 (2013) 1-7. https://doi.org/10.1016/j.fct.2013.03.048.

[76] A.A. Khalaf, W. Ahmed, W.A. Moselhy, B.R. Abdel-Halim, M.A. Ibrahim, Protective effects of selenium and nano-selenium on bisphenol-induced reproductive toxicity in male rats, Hum. Exp. Toxicol. 38 (2019) 398-408. https://doi.org/10.1177/0960327118816134.

[77] N.M. Shafik, M.M. El Batsh, Protective effects of combined selenium and Punica granatum treatment on some inflammatory and oxidative stress markers in arsenic-induced hepatotoxicity in rats, Biol. Trace Elem. Res. 169 (2016) 121-128. https://doi.org/10.1007/s12011-015-0397-1.

[78] A.L. Stefanson, M. Bakovic, Dietary Regulation of Keap1/Nrf2/ARE Pathway: Focus on Plant-Derived Compounds and Trace Minerals, Nutrients 6 (2014) 3777-3801. https://doi.org/10.3390/nu6093777.

[79] C. Zhang, J. Lin, J. Ge, L.-L. Wang, N. Li, X.-T. Sun, H.-B. Cao, J.-L. Li, Selenium triggers Nrf2-mediated protection against cadmium-induced chicken hepatocyte autophagy and apoptosis, Toxicol. in Vitro 44 (2017) 349-356. https://doi.org/10.1016/j.tiv.2017.07.027.

[80] T.-J. Hsieh, P.-C. Hsieh, Y.-H. Tsai, C.-F. Wu, C.-C. Liu, M.-Y. Lin, M.-T. Wu, Melamine Induces Human Renal Proximal Tubular Cell Injury via Transforming Growth Factor-β and Oxidative Stress, Toxicol. Sci. 130 (2012) 17-32. https://doi.org/10.1093/toxsci/kfs231.

[81] G. Salvesen, Program in apoptosis and cell death research, The Burnham Institute, Chem. Rev 102 (2002) 4489-4500.

[82] A.R. Hashim, D.W. Bashir, N.A.E. Yasin, M.K. Galal, E.-G.S. M, Ameliorative effect of N-acetylcysteine against glyphosate-induced hepatotoxicity in adult male albino rats: histopathological, biochemical, and molecular studies, Environ. Sci. Pollut. Res. 28 (2021) 42275–42289. https://doi.org/10.1007/s11356-021-13659-2.

[83] A. Albihn, J. Lovén, J. Ohlsson, L.M. Osorio, M. Henriksson, c-Myc-dependent etoposide-induced apoptosis involves activation of Bax and caspases, and PKCdelta signaling, J. Cell. Biochem. 98 (2006) 1597-1614. https://doi.org/10.1002/jcb.20816.

[84] A.J. Yiu, C.-L. Ibeh, S.K. Roy, B.C. Bandyopadhyay, Melamine induces Ca2+-sensing receptor activation and elicits apoptosis in proximal tubular cells, Am. J. Physiol. Cell Physiol. 313 (2017) C27-C41. https://doi.org/10.1152/ajpcell.00225.2016.

[85] X. Yuan, Z. Fu, P. Ji, L. Guo, A.O. Al-Ghamdy, A. Alkandiri, O.A. Habotta, A.E. Abdel Moneim, R.B. Kassab, Selenium Nanoparticles Pre-Treatment Reverse Behavioral, Oxidative Damage, Neuronal Loss and Neurochemical Alterations in Pentylenetetrazole-Induced Epileptic Seizures in Mice, Int J Nanomedicine 15 (2020) 6339-6353.https://doi.org/10.2147/ijn.s259134.

[86] H.A. Fahmy, A.S. Abd El Azim, O.A. Gharib, Protective Effects of omega-3 fatty acids and/or Nano-selenium on Cisplatin and Ionizing radiation induced liver toxicity in rats, Indian J. Pharm. Educ. Res. 50 (2016) 649-655. https://doi.org/10.5530/ijper.50.4.17.